DPST-80-128-4

^{238}Pu FUEL FORM PROCESSES QUARTERLY REPORT

OCTOBER - DECEMBER 1980

E. I. du Pont de Nemours & Co.
Savannah River Laboratory
Aiken, SC 29808

PREPARED FOR THE U. S. DEPARTMENT OF ENERGY UNDER CONTRACT DE-AC09-76SR00001

DISCLAIMER

DPST-80-128-4

^{238}Pu FUEL FORM PROCESSES QUARTERLY REPORT

OCTOBER - DECEMBER 1980

Approved by:

R. L. Folger, Research Manager
Hydrogen and Ceramic Technology Division

Publication Date: August 1981

E. I. du Pont de Nemours & Co.
Savannah River Laboratory
Aiken, SC 29808

PREPARED FOR THE U. S. DEPARTMENT OF ENERGY UNDER CONTRACT DE-AC09-76SR00001

page blank

CONTENTS

page blank

FOREWORD

This report is one of a series to summarize progress in the Savannah River Laboratory ^{238}Pu Fuel Form Program. This program is supported primarily by the DOE Advanced Nuclear Systems and Projects Division (ANSPD).

Goals of the Savannah River Laboratory (SRL) program include providing technical support for the production of $^{238}PuO_2$ fuel forms in the Savannah River Plant's (SRP) Plutonium Fuel Form (PuFF) Facility. This part of the program includes:

Demonstration of processes and techniques developed by the Los Alamos National Laboratory (LANL) for production at SRP. Information from the demonstration will provide the technical data for technical standards and operating procedures.

Technical Support to assist plant startup and to ensure continuation of safe and efficient production of high-quality heat-source fuel.

Technical Assistance after startup to accommodate changes in product and product specifications, to assist user agencies in improving product performance, to assist SRP in making process improvements that increase efficiency and product reliability, and to adapt plant facilities for new products.

page blank

MULTI-HUNDRED WATT (MHW) PROCESS SUPPORT

IMPACT RESPONSE OF SRP MHW $^{238}PuO_2$ FUEL SPHERES

Summary

The iridium containment shell of an encapsulated SRP fuel sphere, Multi-Hundred Watt Fuel Test (MHFT) 65 split open during a Safety Verification Impact Test (SVT), and about 2 g of $^{238}PuO_2$ was released (Figure 1). (Typical oxide releases in previous tests were 1 to 10 mg). The cause of the impact failure was investigated by an interagency task force organized by the Department of Energy (DOE). According to the scenario generally accepted by the task force, (1) the iridium cladding sustained a "lobe-type push-through" deformation failure (Figure 1), (2) cladding deformation was caused by the shearing of large, "hard" (fracture-resistant) chunks of fuel, accompanied by the inability of the embrittled iridium to withstand the strain imposed upon it during fuel fracture, and (3) the iridium embrittlement and failure was, in turn, the result of its high phosphorus content.

Concern arose over the task-force-proposed failure mechanism for MHFT 65 (SRP Shpere 18) for the following reason: if push-through failure were caused by shear of large pieces of fuel along pre-existing cracks, later production spheres might be more susceptible to failure because they were more crack-resistant and should break up on handling and storage into fewer but larger and "harder" chunks. Impact results for SVTs would then be strongly dependent on sphere orientation (and hence crack orientation) with respect to the impact face so that uncertainty on how to weight the tests for impact response would remain, and the probability of more failures of the type sustained by MHFT 65 could not be assessed.

After the available data were reanalyzed independently by the Savannah River Laboratory (SRL), SRL concluded that lobe-type push-through failure of MHFT 65 was not caused by shear of large, hard chunks of fuel but rather by an alternative mechanism involving extrusion, i.e. "sandbagging", of the iridium and fuel into a radial split in the graphite impact shell (GIS) that surrounds the iridium-clad fuel sphere. SRL also concluded that the inability of the iridium cladding of MHFT 65 to withstand the strain it underwent during fuel fracture did result from the embrittlement imparted to it by its high phosphorous content. Therefore, the

impact response of all SRP fuel spheres is expected to be about the same. SVTs conducted to date at LANL support this prediction, since no recurrence of the behavior shown by MHFT 65 has occurred and no unexpected failures have taken place.

Although the SVT results and the SRL-proposed failure mechanism do not discount the failure of MHFT 65 or predict the probability of recurrence, they do suggest that (1) failure of MHFT 65 was a rare event; and (2) observed behavior of fuel spheres during SVT is typical of the behavior expected of all SRP fuel because impact response should not be significantly orientation- or production-history-dependent.

The failure mechanism proposed for MHW spheres is expected to be relevant for GPHS pellets. The application of the mechanism to GPHS fuel depends upon (1) the orientation of the fuel at impact (e.g., side-on versus end-on) and (2) the similarity of the GIS materials of GPHS to those of MHW. For side-on impact of a GPHS pellet (the expected impact orientation), the impact scenario described in this report for MHW may be a valid first approximation because both impacts have a circular profile in the Y-Z plane (vertical plane perpendicular to the longitudinal pellet axis). For side-on impacts, then, any lobe-type failure of iridium in GPHS fuel should be the result of failure of the GIS rather than of effects of pre-existing crack networks in the fuel. For end-on or near end-on impact of a GPHS pellet, the MHW impact model is not expected to be valid.

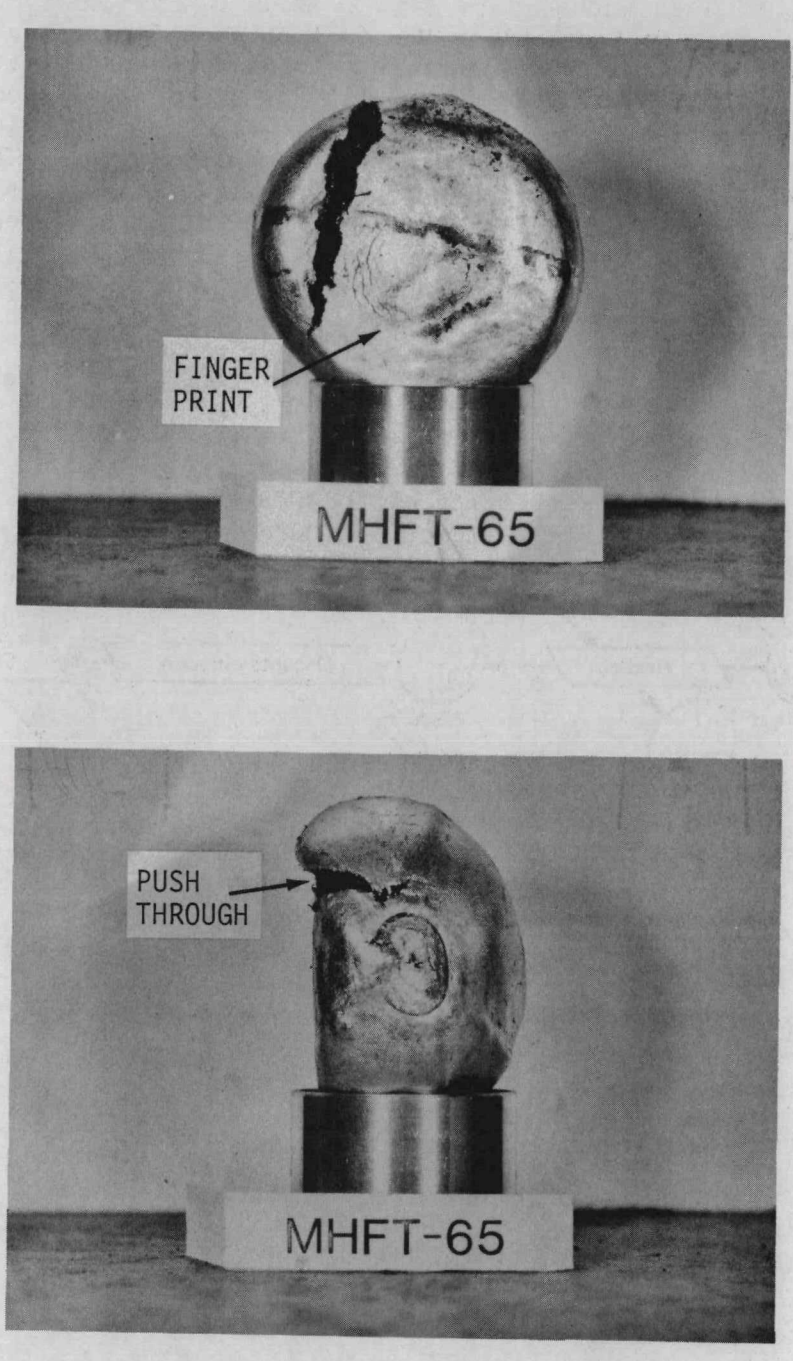

FIGURE 1. Impact Face and Profile of MHFT 65 (Photographs courtesy of D. Pavone, LANL[1]).

Description of Fuel Form and Test Conditions

The sequence for assembling MHW fuel spheres for service in a radioisotopic thermoelectric generator (RTG) is shown schematically in Figure 2. A $^{238}PuO_2$ sphere fabricated in the Plutonium Fuel Form (PuFF) Facility at SRP is encapsulated in thin iridium hemispheres called post-impact containment shells (PICS). The encapsulated fuel, or post-impact sphere assembly (PISA), is then placed in a graphite impact shell (GIS). The GIS is designed to sufficiently absorb the shock of an impact of the space vehicle with Earth's surface. If a mission failure necessitates re-entry of the space vehicle, the vehicle-earth impact would not cause the fuel to breach the PICS and contaminate the biosphere. The final assembly of a PISA within a GIS is called a fuel sphere assembly (FSA). Twenty-four FSAs are assembled as shown in Figure 3 into an RTG.

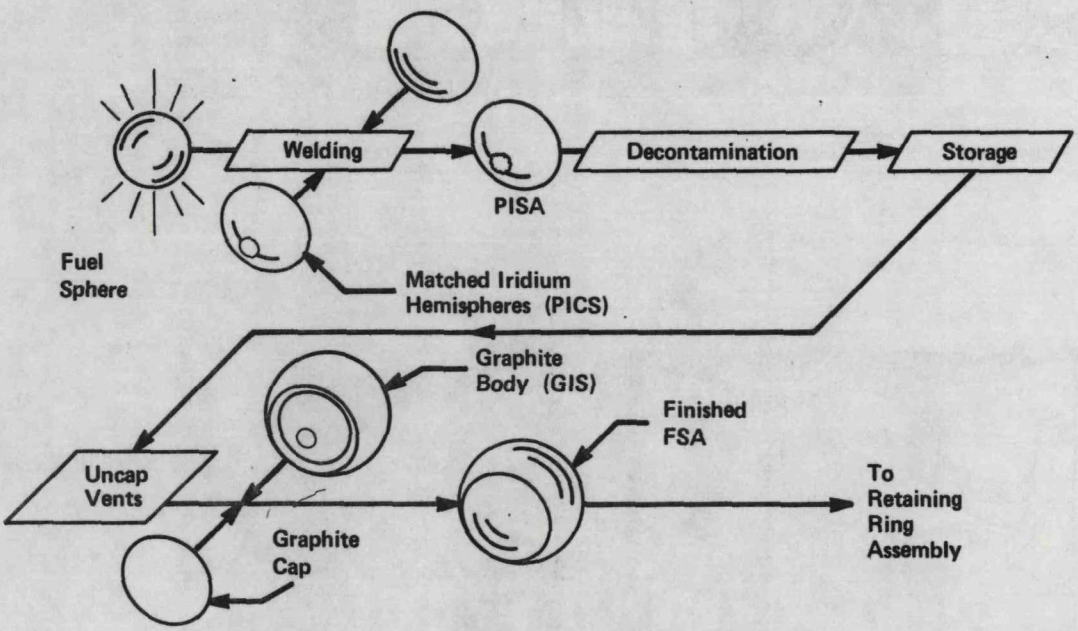

FIGURE 2. Sequence of Assembling FSA[2]

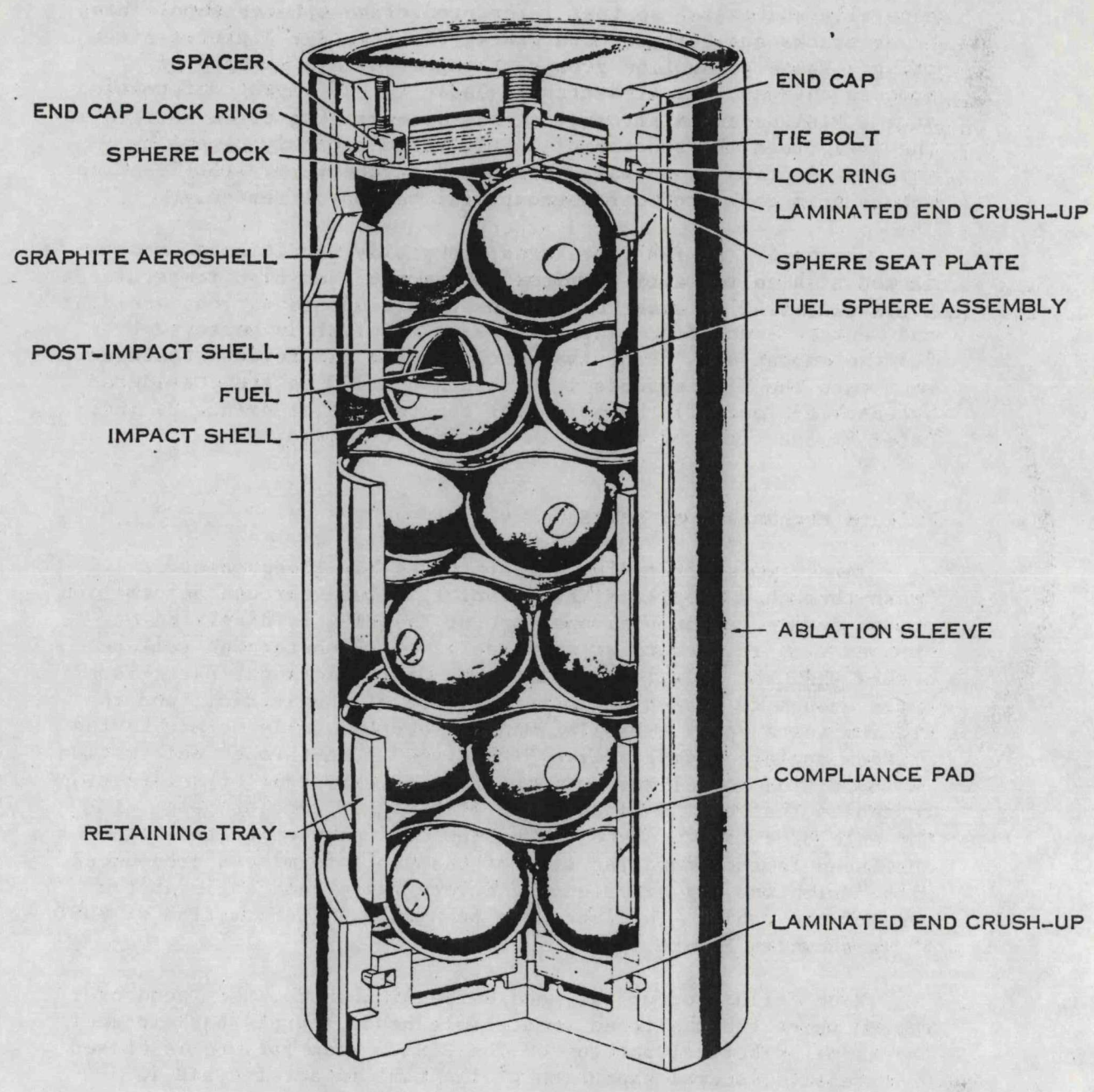

FIGURE 3. Core of MHW Radioisotopic Generator[2]

SRP sphere production can be divided into four groups according to modifications made in the production flowsheet in attempts to make more crack-resistant spheres. These efforts were generally successful so that later production spheres should have fewer cracks and larger, more crack-free ("harder") pieces after aging. These production groups, together with a summary of process changes, are presented in Table 1. If impact deformation of the PISA depended strongly on the pre-existing crack pattern in the fuel, then the success of an SVT would probably depend on which production group was represented in the test. (At least one sphere from each production group will be impact tested.)

During SVT's, FSA's are aged, thermally conditioned, and impacted at high velocity (typically 85 m/sec) and high temperatures (typically 1440°C) under conditions that simulate various accident and reentry scenarios. The success of the test is measured by (1) the amount of $^{238}PuO_2$ that escapes from the iridium containment into the GIS (amounts less than about 100 mg are considered acceptable), and (2) the potential for release of oxide, as indicated by the sizes of cracks in the iridium cladding.

Failure Mechanisms of MHW Spheres

Three types of iridium failure modes have been observed: "push-through," hoop, and "fingerprint." Push-through deformation occurs during impact when one part of the PISA is displaced or sheared with respect to an adjacent part. Push-through failure occurs when the relative displacement of the adjacent parts is large enough to exceed the plastic limit of the iridium, and the iridium tears apart. Displacement is approximately normal to the iridium surface A distinctive "lobe type" push-through deformation is identified as follows: The profile of this type of deformation resembles that of the impact face of a bag of sand dropped onto the edge of a table. Here the unsupported portion of the bag continues farther down the side of the table forming a pronounced "lobe" with the bag experiencing a very sharp bend angle at the edge of the table. The lobe type push-through deformation of MHFT 65 is shown in Figure 1.

Hoop failure occurs at, and perpendicular to, the "bend over" region where the flattened impact face bends sharply back to meet the normal spherical portion of the PISA. Hoop failure is caused by excessive lateral expansion of the time impact fce and is similar to the cracks that develop perpendicular to the equator when a clay ball is squashed. Hoop failures have not been observed in SRP SVT's.

Fingerprint cracks are intergranular cracks that form on the impact face of the iridium in roughly concentric circules resembling a fingerprint. Typically, fingerprint cracks do not penetrate the wall thickness of the iridium and are usually not considered serious.

TABLE 1

SRP Sphere Production Groups

Group	SVT No	Sphere No	Approximate Relative* Fracture Resistance	General Production Conditions
1	67 68 69 70 71	33 thru 53	1	Parabolic hot press load ramp. T = 1575°C or more (T is maximum hot press temperature). P = 3000-3400 lb force (P is maximum hot press pressure).
2a	72	54 thru 70	2.5	Linear hot press load ramp. T ≅ 1575°C more consistently. P = 2500 lb force. Reoxidized in cell atmosphere.
3	73	71 thru 81	1	Reoxidized in flowing O_2 in final heat treat furnace at ambient temperature versus reoxidize in cell atmosphere (rapid versus slow reoxidation).
2b	74	82 thru 132	2.5-3.0	Reoxidize in cell atmosphere for 24 hours. T ≅ 1550°C starting Sphere 85; otherwise similar to Group 2a.
4	75 76	133 et seq	2.7-3.0	>103.5-watt spheres versus 102-102.5-watt spheres previously. Density increased 1-2% TD. Longer hot press time. Pressure held during cooldown. Spheres 133-139 transition period.

* On a scale of 1-3, with 1 being lowest.

Failure of FSA Containing Sphere MHFT 65

The encapsulated fuel sphere in MHFT 65 failed catastrophically, according to a post-SVT examination conducted during September 1979. A large crack (4 cm long x 4 mm wide) opened in the iridium (PICS) spilling 2.1 g (versus 1 to 10 mg for previous tests) of $^{238}PuO_2$ into the GIS surrounding the PICS. If this undesirable result were typical of those obtained from production sphere SVT's, the biological hazard source term for the safety analysis using SRP-produced spheres and the ORNL iridium alloy would increase by a factor of between 10 and 100 over that used for earlier Mound Facility spheres. A higher biological source term creates concern not only for the flight worthiness of the MHW fuel already produced for Galileo Missions, but also for the GPHS fuel being developed for the International Solar Polar Mission.

MHFT 65 was aged at 1210°C (typical, see Table 2) for 4400 hr (longer than most) and impacted at 1440°C and 85 m/sec (both typical). It was the third sphere clad in DOP 26 iridium. The phosphorus content (as measured by Auger spectroscopy) of the aged PICS of MHFT 65 was substantially greater than that of any other PICS measured including one that had aged longer.

Explanation of Failure by Interagency Task Force

- The mechanism of failure of MHFT 65 generally accepted by the task force was that of lobe-type push-through deformation caused by shearing of large, hard chunks of fuel while the iridium was unable to withstand the strain because of the embrittlement resulting from the high phosphorus content of the iridium alloy. Evidence for lobe-type push-through deformation occurring from the shear of large chunks came primarily from two impact tests, MHFT 61 and 70, neither of which was a failure.

1. Shear planes observed in MHFT 61 (Figure 4b) ran from the center axis (perpendicular to the impact face) of the impacted sphere toward the push-through area of the impact face. These planes formed nearly an isosceles triangle with the triangle's base along the impact face, and the triangle's apex along the center axis about two-thirds to three-fourths of the distance from the impact face to the rear of the sphere. The left-hand shear plane appeared to correspond with a large crack observed by radiography of the sphere before impact (Figure 4a). The task force postulated that as rate of movement of material below these planes decreased, large chunks above the planes slid along the planes and sheared the iridium PICS.

2. Dislocation of the iridium along a shear plane from the back of MHFT 70 to the point of potential push-through suggested

motion of a single sphere piece (Figure 5). The impact behavior of MHFT 70 was postulated to indicate that push-through deformation can result when pieces of fractured fuel move either as large masses, or as many small pieces acting in concert along a single fracture plane.

- Phosphorus decreases the ductility of iridium and therefore could contribute to impact failures.

- Overall, the FSAs using LANL-SRL type fuel and new doped iridium (HD and DOP 26) alloy show better impact responses than do Mound Facility fuel and undoped iridium originally used (Table 2) when impact responses of fuel spheres are compared. (In Table 2 MHFT 65 is counted as a single event and is not weighted according to severity.) Table 2 shows, that in terms of number of events, the new fuel-iridium system has no hoop strain failures and fewer push-through failures.

- More SVT data are needed on production fuel to provide bases for assessment of the safety of SRP fuel. The actual performance of flight-quality SRP fuel with DOP 26 iridium FSAs is not known at this time. Even though the total number of impacted spheres having the LANL-SRP type fuel and new doped iridium alloys is assuming statistical significance, each test has had differences in fuel fabrication, storage time, test conditions, etc., so that there is no statistical set of impact data on flight-quality hardware (SRP fuel with DOP 26 iridium). Because of these differences, the probability of recurrence of a large crack cannot be accurately assessed.

- There are insufficient data to disqualify Sphere MHFT 65 at this time.

TABLE 2

LANL-Fueled MHW Impact Test Summary Prepared for MHFT Task Force

Sample No.	Fuel	Velocity, fps	Temp., °C	Aging Conditions		Hoop Strain	Failure Type*			Iridium Lot
				Time, hr	T, °C		Hoop	Fingerprint	Fuel Push-Through	
MHFT-2	MF	274	1374	18	1500	0.065		No failure		4A, 4A
MHFT-3	MF	276	1365	18	1500	0.134	x	-	-	5, 5
MHFT-4	MF	279	1375	18	1500	0.081	x	x	-	5, 4A
MHFT-12	MF	286	1480	18	1500	0.088	x	-	-	15B, 13
MHFT-26	MF	247	1550	833	1272	0.147	-	x	-	51, 50
MHFT-27	MF	249	1550	833	1272	0.043	-	-	x	-
MHFT-29	MF	253	1093	720	1265	0.059	x	x	x	51, 51
MHFT-30	MF	250	1550	720	1265	0.045	-	x	-	51, 52
MHFT-31	MF	243	1550	720	1265	0.039	-	-	x	44, 44
MHFT-32	MF	285	1370	0	0	0.075		No failure		EI-III
MHFT-33	MF	282	1370	0	0	0.066		No failure		EI-III
MHFT-34	MF	284	1375	18	1500	0.056		No failure		WC
MHFT-35	MF	281	1375	18	1325	0.066	-	x	x	WC
MHFT-36	MF	280	1375	18	1325	0.069	-	x	x	WC
MHFT-39	MF	284	1100	2009	1207	0.061	x	-	x	WC, n
MHFT-40	MF	224	1440	2009	1214	0.038	-	-	x	WC, n
MHFT-45	MF	279	1440	720	1214	0.083	-	x	x	EI-III
MHFT-47	MF	281	1440	720	1214	0.073	-	-	x	WE
MHFT-48	MF	285	1440	720	1214	0.133	x	x	-	WE
MHFT-49	MF	286	1100	720	1214	0.051	x	x	-	WE
MHFT-50	MF	281	1440	731	1205	0.116	-	x	x	EI-III
MHFT-54	MF	280	1440	756	1208	0.100	x	-	x	WG
MHFT-55	MF	285	1440	777	1214	0.091	-	-	x	HD
MHFT-56	MF	284	1440	777	1214	0.066	x	x	-	HD
MHFT-57	MF	283	1440	4000	1215	0.091	-	x(?)	-	HD
					Percent failed		40	48	48	
MHFT-58	LANL	281	1440	737	1210	0.081		No failure		HD
MHFT-59	LANL	283	1440	737	1210	0.050		No failure		HD
MHFT-60	LANL	276	1440	4423	1210	0.080	x weld	-	x((?)	HD
MHFT-61	SR-2	243	1440	8834	1210	0.069	-	No failure	-	DOP-26
MHFT-62	SR-11	279	1440	720	1210	0.124	-	x	x	HDR
MHFT-64	SR-17	279	1300	720	1210	0.108	-	x	-	DOP-26
MHFT-65	SR-18	279	1440	4400	1210	0.080	-	x	x	DOP-26
MHFT-66	SR-23	279	1440	720	1210	0.069	-	No failure	-	HD
MHFT-67	SR-36	272	1440	100	1200	0.074	-	-	-	DOP-26
					Percent failed		11	33	33	

* x = Failure confirmed
- = No evidence of failure

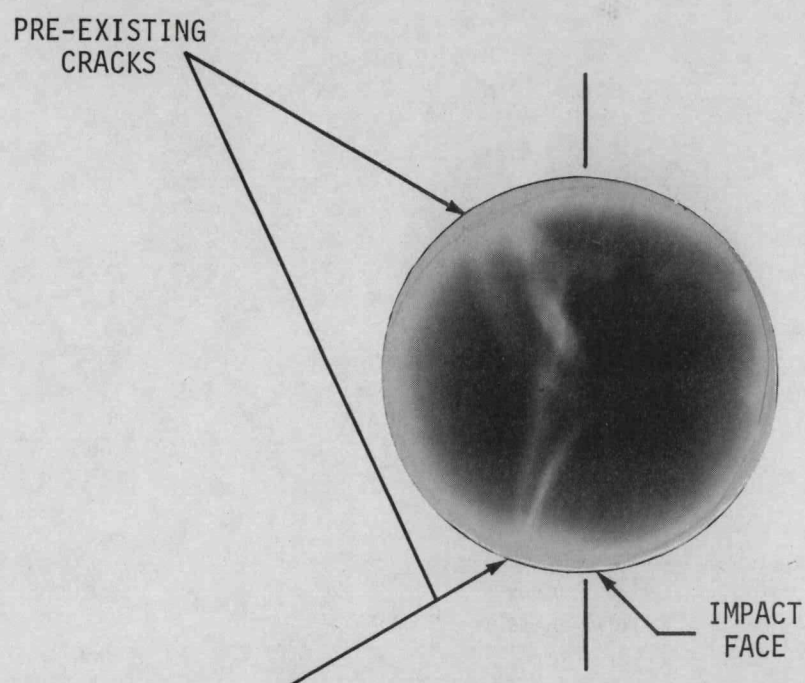

a. Radiograph of FSA Before Impact

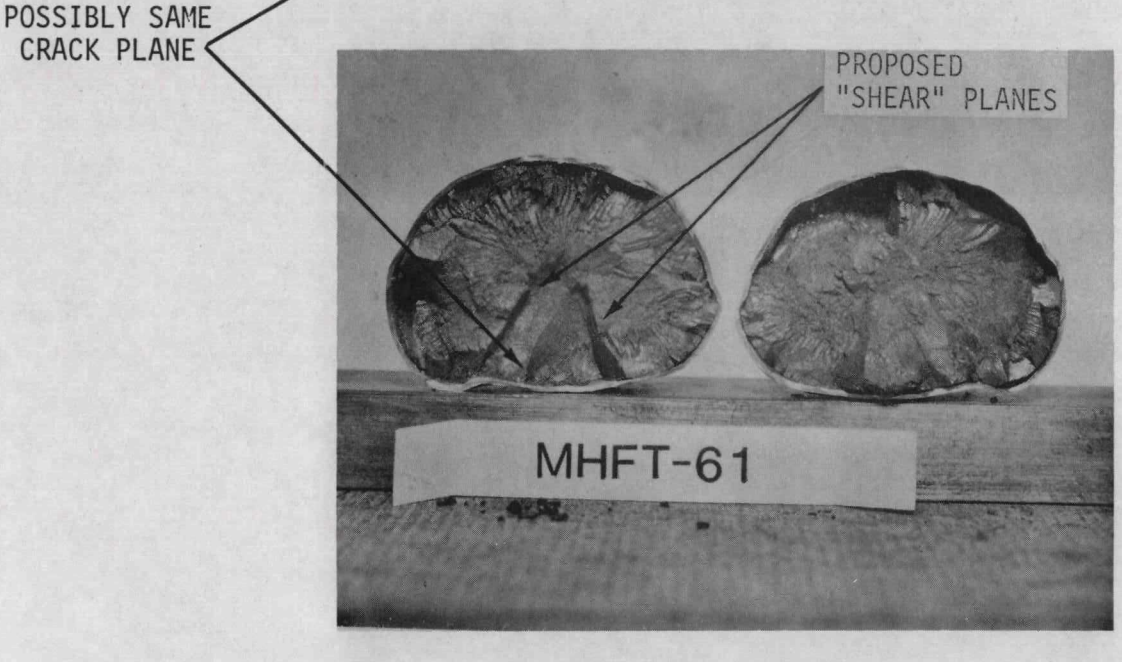

b. Section After Impact

FIGURE 4. SRP Test MHFT 61 (Photographs courtesy of D. Pavone, LANL[3])

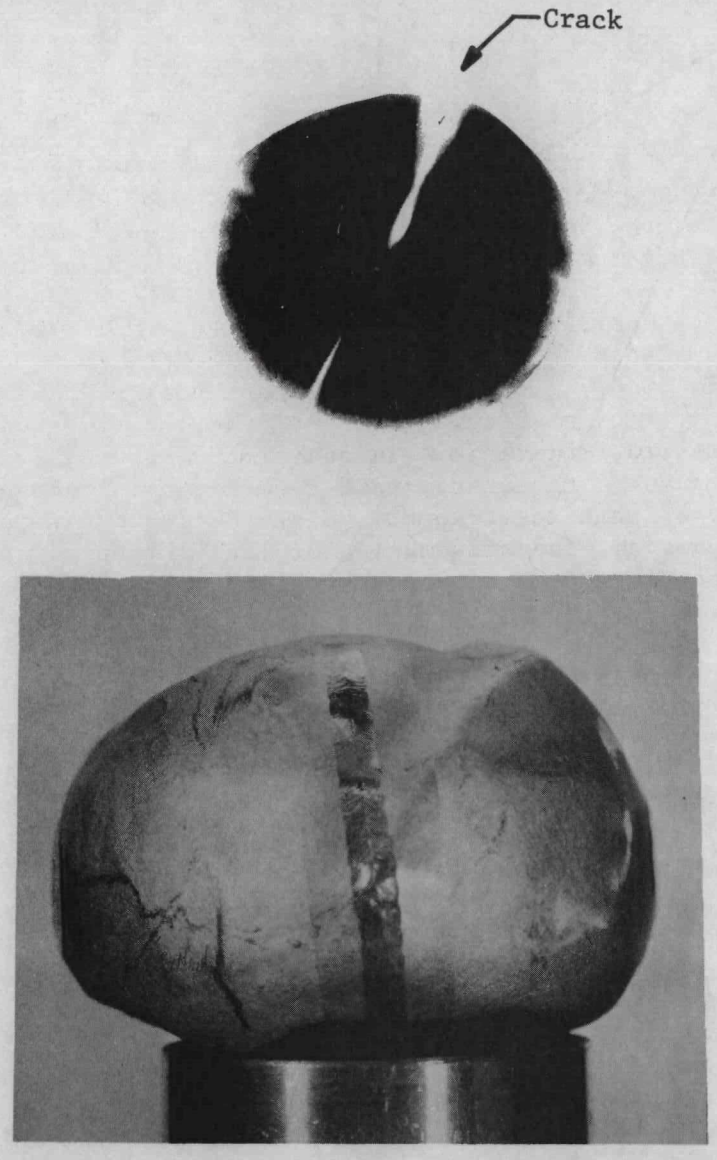

FIGURE 5. Impact of MHFT 70. Deformation from shear of two halves of sphere; no push-through failure. (Photographs courtesy of D. Pavone, LANL[4]).

SRL Evaluation of Failure of FSA Containing MHFT 65

SRL believes the following evidence argues against lobe-type push-through being caused by shear of large chunks of fuel.

Photograph of Impacted FSA MHFT 61. MHFT 61 showed lobe-type deformation but no breach of the Ir. Shear planes are symmetrical around the center axis of MHFT 61 (see Figure 4), but push-through deformation occurs only along one plane. There should be an equivalent shearing deformation along the other plane. Also, the apex of the shear plane is not at the back surface of the sphere, but in the body; i.e., the shear plane does not seem to extend all the way through as would be the case for shear of a large chunk or mass along the plane (MHFT 70, Figure 5). In addition, the crack seen in the radiograph appears to correspond better to a different crack plane (see Figure 4) than to the shear plane leading into the push-through. However, the orientation of the radiograph may not be known accurately enough to allow such a distinction.

Lack of Prominent Lobes on MHFT 70. MHFT 70 showed that deformation can occur by sliding of large masses, but that lobe-type push-through deformation does not necessarily occur as the result. Pre-impact radiographs of MHFT 70 (Figure 5) showed that the sphere was completely separated into two hemispheres along a flat pole-to-pole plane with the fracture plane oriented in the same direction with respect to the impact face as the deformation line shown in Figure 5. However, MHFT 70 did not experience a lobe-type push-through deformation and did not fail.

PuFF records show that the sphere (SRP Sphere 39) used in MHFT 70 had fractured prior to gauging and had to be reassembled when it was loaded into the PICS for welding. This fracture gave rise to the very large separation of two hemispheres seen in the radiograph. The fact that the two halves appeared physically separated in the radiograph, and had been reassembled, suggests they may have been kept apart by small particles and asperities which would have helped the two pieces slide over one another.

The condition of SRP Sphere 39 is expected to be unusual for spheres fabricated after SRP Sphere 53, since these later spheres (1) usually remained intact during encapsulation and (2) did not show the tendency to break into hemispheres or quarters along smooth planes that was shown by SRP Spheres 35-53, which did break. Further, MHFT 70 is expected to be unusual because MHFT 67, 68, 69 (SRP Spheres 36, 37, 38) did not deform in the manner of MHFT 70, yet they are sister spheres from the same production group.

Bases for "Sandbagging" Failure Mechanism

Lobe-type push-through deformations of the PICS of the magnitude observed in MHFT 61 and MHFT 65 are not possible without failure of the GIS first. The hypothesis that the shear of large fuel pieces (without failure of the GIS first) causes lobe-type push-through is understood to mean that the pieces of fuel shear over each other and push through the iridium before the iridium contacts the GIS at the point of push-through; otherwise, without failure of the GIS, push-through could not occur. Evidence against this hypothesis is provided by FSA geometry and computer modeling of impact[5].

From the geometry of the FSA at the instant of impact, it can be shown that the radial gap between the PISA and the GIS at the point where the push-through was observed for MHFT 61 is less than the estimated radial displacement observed so that the displacement could not have occurred without deformation or failure of the GIS.

Figure 6a shows the geometry of the FSA at the moment of contact of the PISA with the GIS. (Deformation of the inner radius of the GIS due to its own impact is considered negligible at this early time.) Points along the PISA circumference corresponding to different d/D (see Figure 6a) ratios used in the computer modeling are labeled w,x,y,z. These same relative points are shown for comparison on the cross section of impacted MHFT 61 (Figure 6b). Point x corresponds very closely with the point of contact of the hypothesized push-through or shear plane of the pieces of fuel. In Figure 7, the calculated radial gap for each point is compared with the maximum radial shear experienced by the push-through in MHFT 61 estimated as shown in Figure 8. Though the radial displacement of MHFT 61 push-through is difficult to determine accurately, it is clearly larger than the radial gap between the GIS and the PISA. Hence, to accommodate the observed displacement, the GIS had to give way.

According to results of computer simulations of impact, the GIS-iridium impact occurs before the fuel-iridium impact at points corresponding to the point of push-through seen in Sphere MHFT 61 and other spheres. Figure 7 shows the geometry of the FSA at the moment of impact and the times of contact for points w,x,y,z around the sphere. At all these points, the fuel does not contact the iridium before the iridium contacts the GIS. Once again, push-through would not be possible without failure of the GIS.

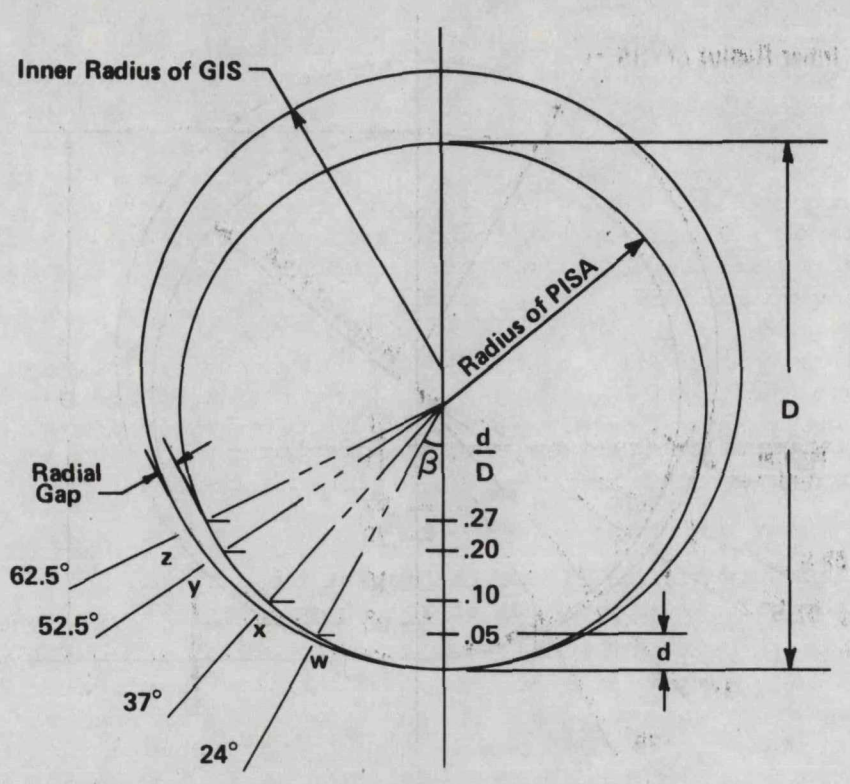

a. Geometry at Instant of Impact of PISA into GIS (Neglecting Small Deformation of GIS Already Started)

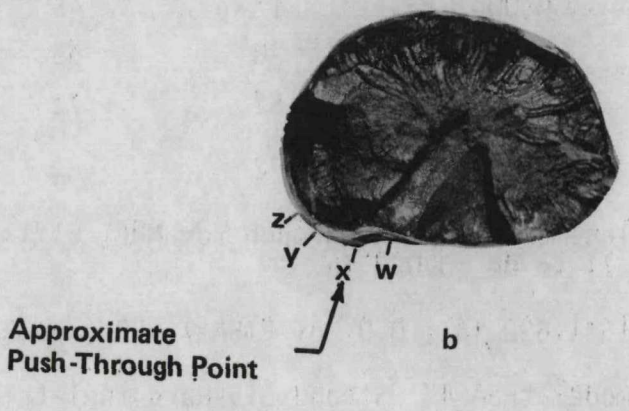

b. Extrapolation of Points w,x,y,z to Impacted MHFT 61

FIGURE 6. Impact Geometry of FSA

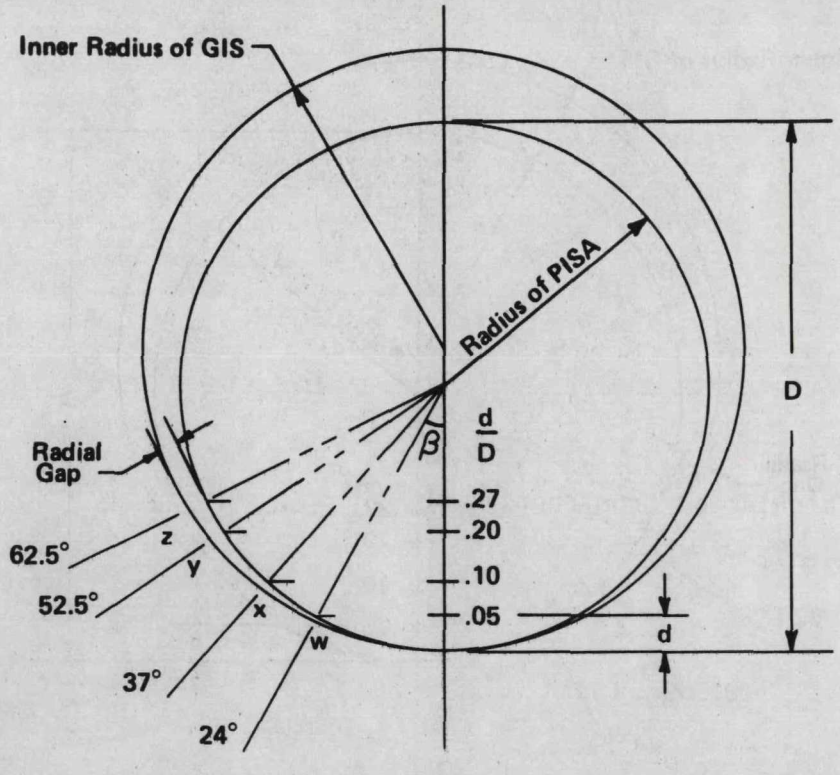

d/D	Initial angle, β	Initial radial gap,* in.	Relative Impact Times** Ir-GIS, μsec	Fuel-Ir, μsec
0.05	24	0.004	17	45
0.10	37	0.009	28	53
0.20	52.5	0.016	52	72
0.27	62.5	0.023	72	83

Maximum radial displacement of push-through for MHFT 61 is estimated from Fig. 11 to be ~0.090 in.

*Based on I.D. of GIS=1.632 in.; O.D. of PISA=1.550 (see Ref. 4).

**Based on computer model "FSA 4": Strong GIS-Hard fuel-friction between GIS-Ir and Fuel-Ir. However, all other computer models (e.g. Strong GIS - Weak fuel - no friction) also showed the same relative impact sequence up to d/D = 0.15 (Ref. 3).

FIGURE 7. Initial Contact Geometry of FSA

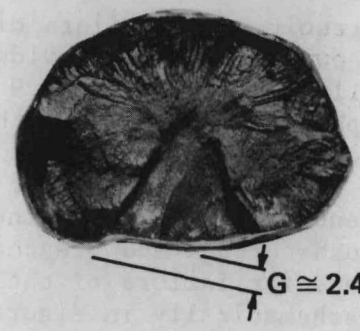

Scale Factor to Reduce G to Actual Size = 0.916

$\therefore G_{Actual} \cong 2.2$ mm = 0.087 in

a. Calculation From Photograph

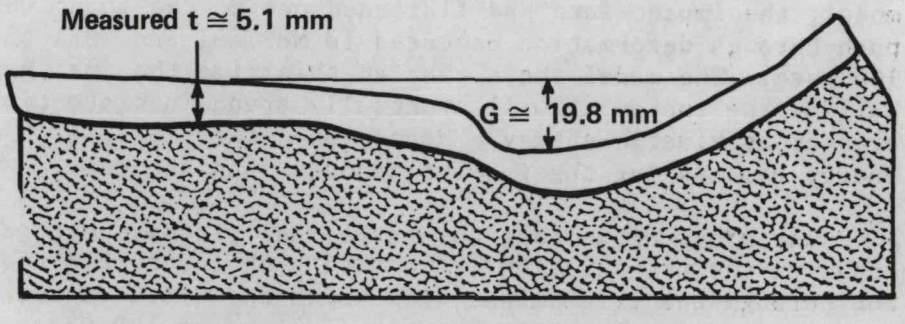

Actual Thickness t of Iridium = 0.024 in

$\therefore$ Estimated Displacement, $G = \frac{19.8}{5.1} \times 0.024 = 0.093$ in

Ave. of both determinations = 0.090 in

b. Calculation From Drawing of Metallographic Mount of Iridium

FIGURE 8. Estimation of Radial Push-Through Deformation of MHFT 61. (Photographs courtesy of D. Pavone, LANL)

The stress required for failure of the GIS, aside from that arising from its own impact, is provided by the lateral expansion of the fuel as illustrated in Figure 9 where the loci of points in an undisturbed sphere are plotted as the sphere deforms during computer-simulated impact. One should remember that the intent of the GIS is to provide restraint for the lateral expansion of the PISA to prevent hoop failure of the iridium. Therefore, where the GIS fails, push-through and breaching of the iridium should be expected. Evidence for failure of the GIS is given in Figure 10a and illustrated schematically in Figure 10b. As shown in Figures 10b and 10c, the proposed mechanism of push-through deformation is failure of the GIS and sandbagging of the fuel into the resultant gap. This mechanism explains the very distinct lobes observed in the push-through. At the inner lip of the gap, very large strains and strain rates would develop, making this point the most probable point of tearing of the iridium as observed in MHFT 65.

The computer simulation of impact shows that at the estimated time of failure of the GIS, the fuel still has sufficient energy to sandbag into the opening in the GIS. Measured total impact time for the FSA was about 200 μsec. According to the computer model, the impact face has flattened out to the point where the push-through deformation occurred in MHFT 61 and MHFT 65 in about 100 μsec. The model shows that at this time the fuel has over half of the energy it will eventually spend in distortion still present as kinetic energy. Hence, when the GIS fails, ample energy remains for the fuel to sandbag into the gap.

One might argue that the large fuel pieces shear across each other on the pre-existing crack with such force that they still cut through the iridium and wedge open the GIS. However, the computer model does not support this. Before 100 μsec, the model shows spallation along the surface of the sphere which would blunt the tips of the pieces. Moreover, the model shows considerable fuel breakup has occurred by 100 μsec so that the large chunks probably no longer exist as such.

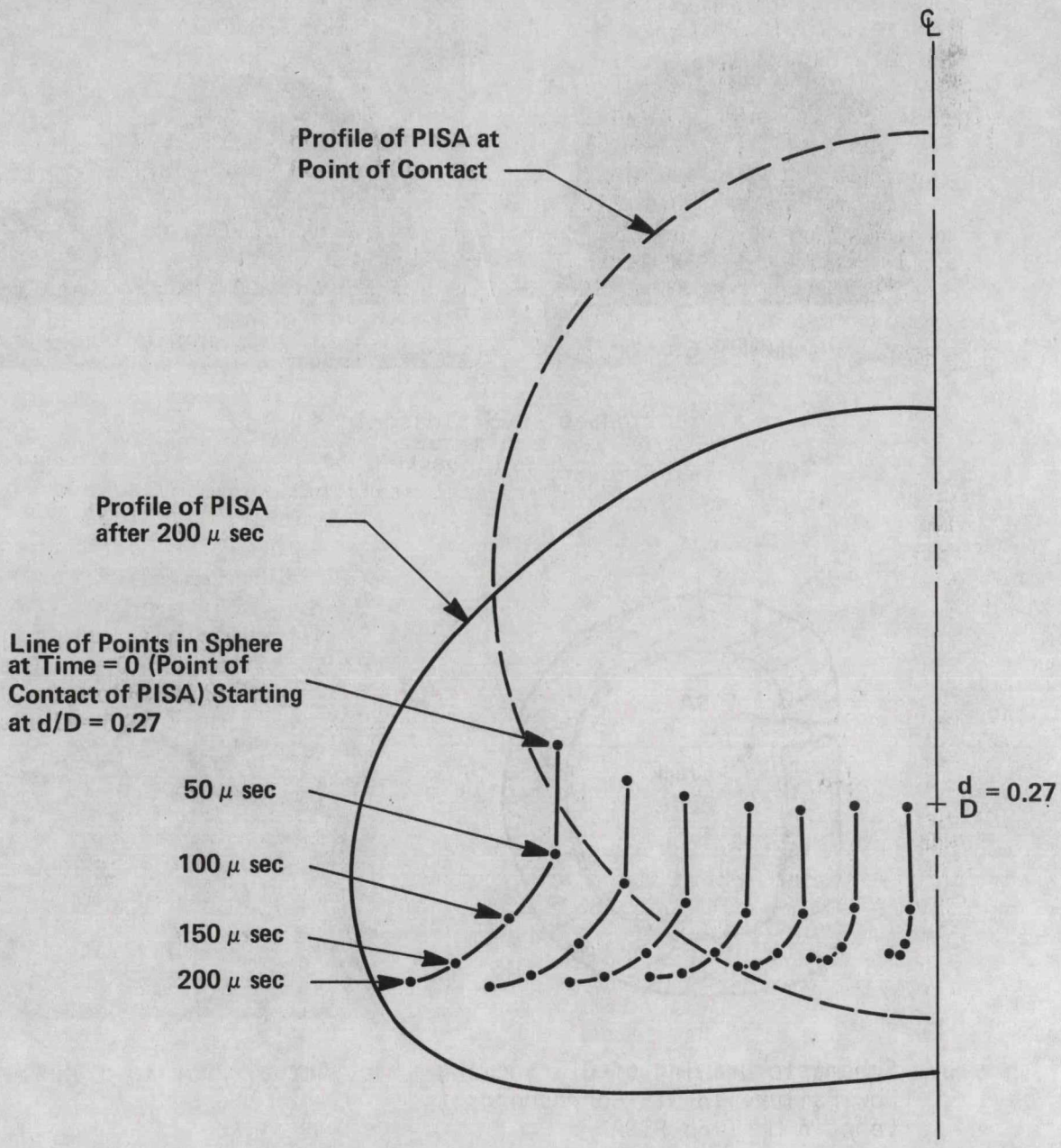

FIGURE 9. Loci of Points in Fuel During Impact Showing Lateral Thrust Near End of Impact[5]

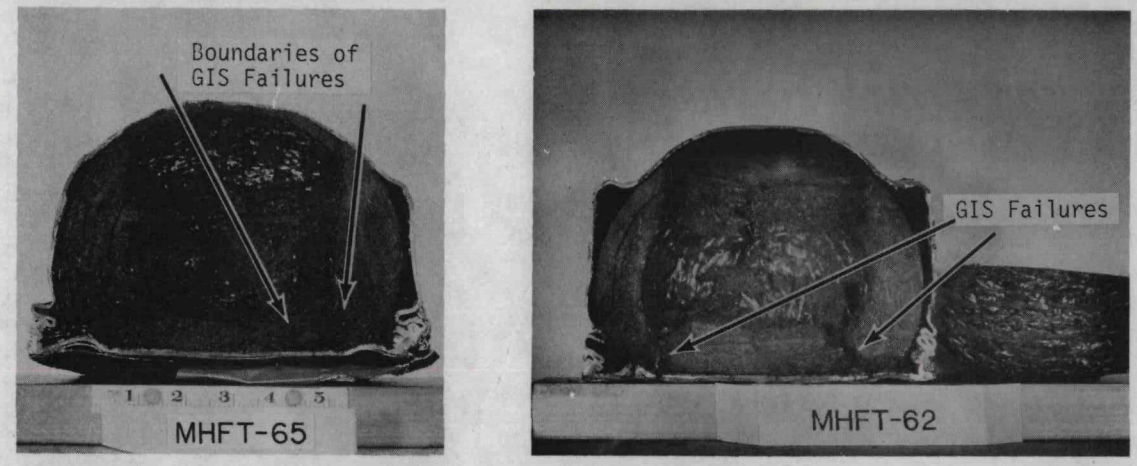

a. Sections of GIS's Used in MHFT 62

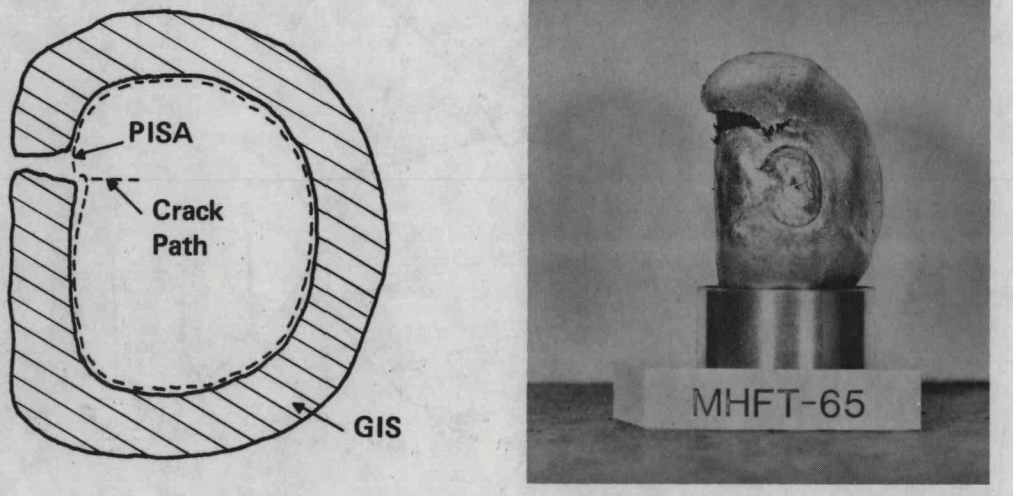

b. Schematic Drawing of GIS Showing How Failure in GIS Corresponds to Lobe in MHFT 65 PISA

c. Actual Profile of MHFT 65

FIGURE 10. Evidence Showing that Push-Through is Caused by Failure of the GIS. (Photographs courtesy of D. Pavone, LANL)

Evidence presented in Figures 6 through 10 indicates that the impact resistance of SRP fuel should not depend strongly on the pattern of large preexisting cracks. FSA impact data indicate that, both from the point of view of the available gap between the iridium and GIS and the relative GIS-iridium and fuel-iridium impact times, lobe-type push-through deformation could not occur unless the GIS also failed. When the GIS fails, we argue that lobe-type push-through occurs by sandbagging of the fuel into the separation in the GIS, not by shearing of large pieces of fuel with respect to each other. The actual profile of cross sections of impacted PISAs and GISs support this mechanism. The mechanism is also supported by SVT behavior of MHFT 70. During this test, a large deformation of the PICS (primarily at the back side) resulted from shearing of two halves of the sphere. The GIS split, but the extent is unknown; the existing photograph of the cross section does not show a split. Therefore, the opportunity for sandbagging of the fuel into a split cannot be assessed. However, the pronounced push-through lobes seen in FSAs containing Spheres MHFT 61 and 65 did not occur, reinforcing the idea that the lobes (which indicate excessive local strain) are the result of fuel sandbagging into the gap of a failed GIS and not due to shear of large pieces along a pre-existing crack.

SVT results on MHW spheres tested so far imply that fractured fuel in SRP Spheres 35-53 may slide easily but no push-through should occur without failure of the GIS. Shear of large chunks along pre-existing cracks is not expected except in the uncommon case where the crack is essentially a smooth flat fracture plane as in the case of MHFT 70. Even then, push-through failure should not occur if the GIS remains intact. For spheres of other production groups (SRP Spheres 54 et seq) fracture planes were not well defined for those that were integral when encapsulated; these spheres should then impact essentially as if they had been integral, i.e., no unusual impact behavior is anticipated. For those spheres that had to be assembled before encapsulation, deformation of the iridium may be more severe, as was the case for MHFT 70, but failure should not occur if the GIS remains intact.

From a discussion of the relationship between cracking patterns and the probability of impact failure, one can infer that impact failure is a function of random variations in the strength of the GIS. Certainly, MHFT 70 showed that substantial lateral thrust by shearing of the fuel pieces does not dominate the rupture tendency of the GIS because the split in the GIS was not noticeably excessive and may have been slight. It is more likely that the cause of GIS rupture is a complex interaction of several impact parameters including GIS strength and fuel lateral thrust. Failure then occurs when the combined effects of these parameters exceed a certain threshold.

Friction and Other Factors as Sources of Statistical Variability of Strain in Iridium

According to SRL's proposed mechanism, failure of MHFT 65 proceeds in two steps: (1) failure of the GIS, and (2) failure of the iridium to accommodate the resultant plastic strain as the fuel pushes into the gap in the GIS. In both steps, there are opportunities for statistical variations in properties that could combine to produce a large failure. In step one of the failure, there could be variations in the strength of the GIS, or variations in the lateral thrust. The latter would depend on how the sphere deformed and this in turn on the strength of the sphere and on other factors as well, such as very large flat fracture planes appropriately oriented. How much the strength varies among the GISs and the spheres is not known nor is it known whether the magnitude of strength variation among spheres is significant compared to the large fracture energy that is available. The role of large pre-existing cracks is usually not first order for the reasons given above.

In step two, several prominent factors that affect the ability of the iridium to withstand the plastic strain can vary considerably. One of the most obvious of these factors is the phosphorus (or possibly other impurity) content. Another is the difference in time between fuel fracture and GIS failure; this would affect the size of the gap in the GIS and the energy available to the PISA to sandbag into it. Variations in these factors cause variations in iridium strain.

Another factor affecting step two that has a large potential for variation is friction at the GIS-iridium and iridium-fuel interfaces. This friction was emphasized in the computer modeling study and may vary widely enough to cause failure or nonfailure at random among FSAs, especially those in which the iridium has a higher phosphorus content. For example, the difference in the calculated hoop strain with and without friction (Figure 11) is large enough to suspect possible effects to occur with variations in friction forces.

The computer simulation of FSA impacts showed that as GIS-iridium and fuel-iridium interfacial frictions increased, the amount of strain in the iridium increased. The increased strain was the result of locking of the iridium between the GIS and fuel so that the motion of the iridium relative to the GIS and the fuel is retarded. Because of this locking, the circumferential (from front around to back) deformation character of the iridium shell is altered and the hoop strains are significantly increased, especially in the region where the flat impact face meets the curvature of the sides of the shell (bendover region). Further, the effect of friction is to cause the circumferential strain to become tensile over most of the front flattened region of the iridium shell. When the coefficient of friction is zero, this strain is calculated by the computer model to be compressive, but becomes increasingly tensile as the coefficient of friction increases. As friction increases, the magnitude of the circumferential strain becomes of the same order as the maximum hoop strains and is largest in the area just before the bendover region begins. Iridium strain rate also changes rapidly as the shell goes from compressive very early in impact to tensile as the impact face flattens out. Iridium is reported to be strain-rate sensitive, with ductility decreasing with increasing strain rate. Differences in friction could arise from differences in the amount of dimpling on the impact face or from the presence of vapor-deposited material on the inside surface of the iridium as has been frequently observed. In one instance in particular (Sphere MHFT 17, an old aged Mound Facility sphere), the fuel had swelled to fill the PICS and adhered tightly to the iridium via a vapor-deposited reaction layer.

In addition to variations in friction, there are also variations in the grain size and phosphorus distribution in the iridium. All of these effects could lead to substantial variability in the impact response of the FSA.

Failure Expectation Based on Failure Mechanism and SVT Results

Failure mechanism proposed by SRL predicts that impact response of all SRP production spheres should be about equal. Impact results to date on all SRP spheres support that prediction.

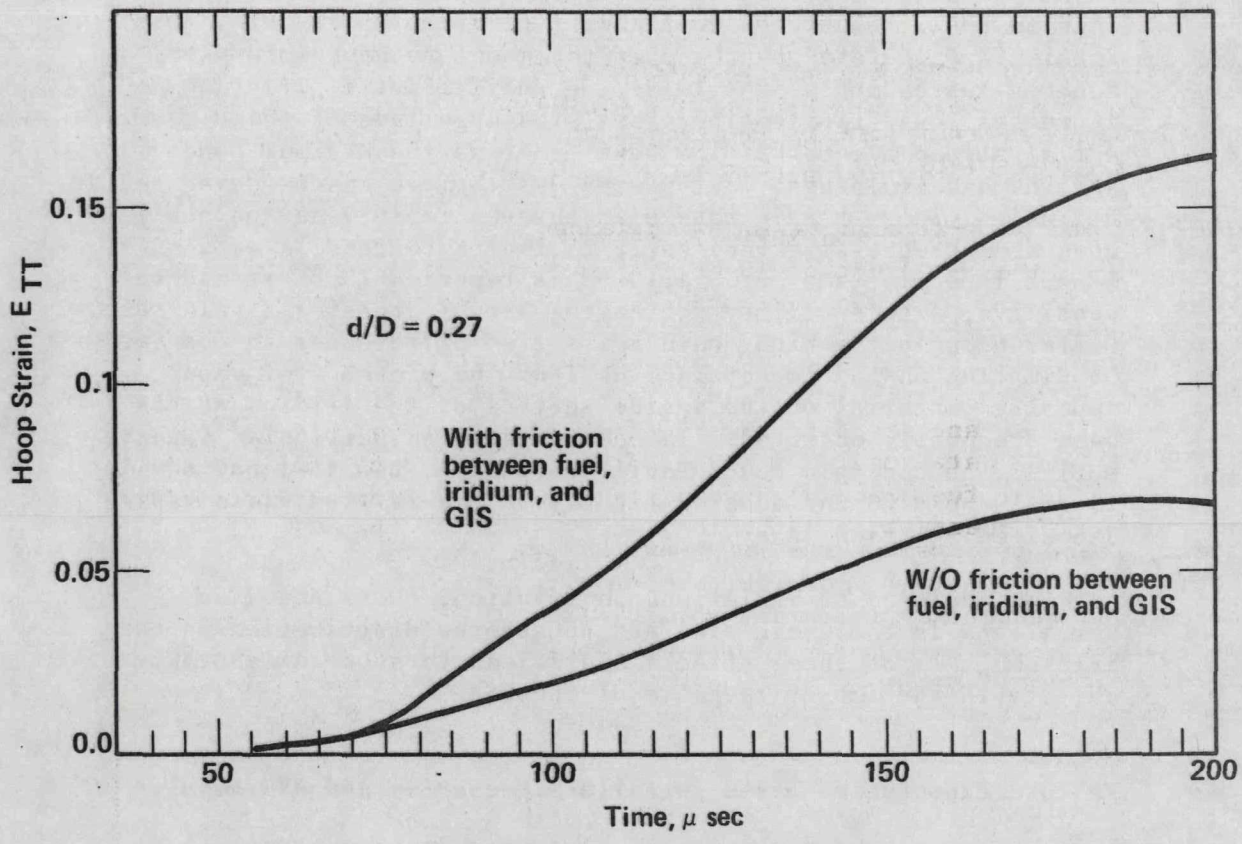

FIGURE 11. Comparison of Hoop Strain-Time Histories in the Iridium Zone[5]

Photographs of all SRP impacted spheres are shown in Figures 1, 12-19. Aging and impact conditions are described in Table 3. Except for MHFT 65, preproduction spheres (MHFT 61-66, Figures 12-15) have shown much the same impact response as did production spheres (MHFT 67-72, Figures 16-20), as expected from the failure mechanism model. Four of the five impacted production spheres have been from the same production group (Group 1, see Table 1). In only one SVT (with MHFT 69), the iridium failed. The failure was attributed to the low impact temperature (Table 3). The fifth SVT was on MHFT 72, which was from Production Group 2a; the iridium did not fail.

With the exception of MHFT 70, the impacted production spheres are similar in appearance. The PISA containing MHFT 70 showed considerable push-through deformation along a plane oriented at 25 degrees to the impact surface. This impact response is not typical of this production group (Group 1) as evidenced by the impact of sisters MHFT 67, 68, and 69 (Figures 16-18).

As of the SVT on MHFT 72, the push-through failure incidence of SRP fuel is 3 out of 10 or 30% (counting MHFT 69 as a push-through and including preproduction spheres). Discounting MHFT 69 (low-temperature impact), the failure rate is 2 out of 9, or 22%, considerably lower than the 45% push-through failure incidence previously experienced for MF fuel (Table 2). Although the probability of another catastrophic failure cannot be calculated, the available data suggest that (1) failure of MHFT 65 was a rare event, (2) fuel impact response is not orientation- or production history-dependent, and (3) the spheres used in the SVTs are representative of SRP fuel. These conclusions are based on (1) low failure incidence of SRP fuel; (2) impact verification to date that, as predicted, spheres from different production groups show the same impact response; and (3) considerations of conditions for catastrophic failure discussed under "Explanation of Failure Mechanisms." SRL recommends completion of planned SVTs to confirm these conclusions.

For side-on impact of GPHS fuel, the impact results are expected to be approximated by the impact response of MHW fuel because of the similar geometry (circular cross section of sphere and cylinder perpendicular to longitudinal pellet axis). Therefore, for side-on impact, GPHS fuel impact response should depend on the GIS strength and not on the product history or pellet crack orientation.

a. Impact Face

b. Profile

FIGURE 12. Impacted MHFT-61. (Photographs courtesy of D. Pavone, LANL[3])

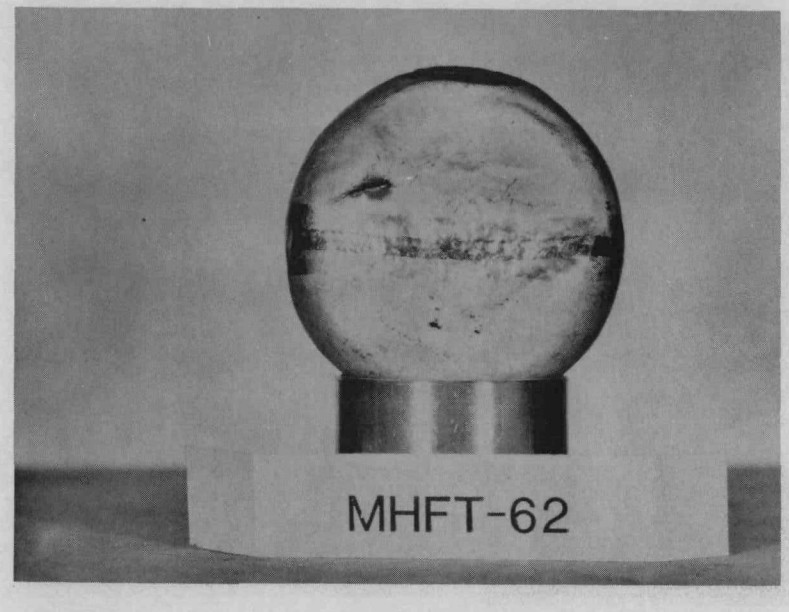

a. Impact Face

b. Profile

FIGURE 13. Impacted MHFT 62 (Photographs courtesy of D. Pavone, LANL[6])

a. Impact Face

b. Profile

FIGURE 14. Impacted MHFT 64. (Photographs courtesy of D. Pavone, LANL)

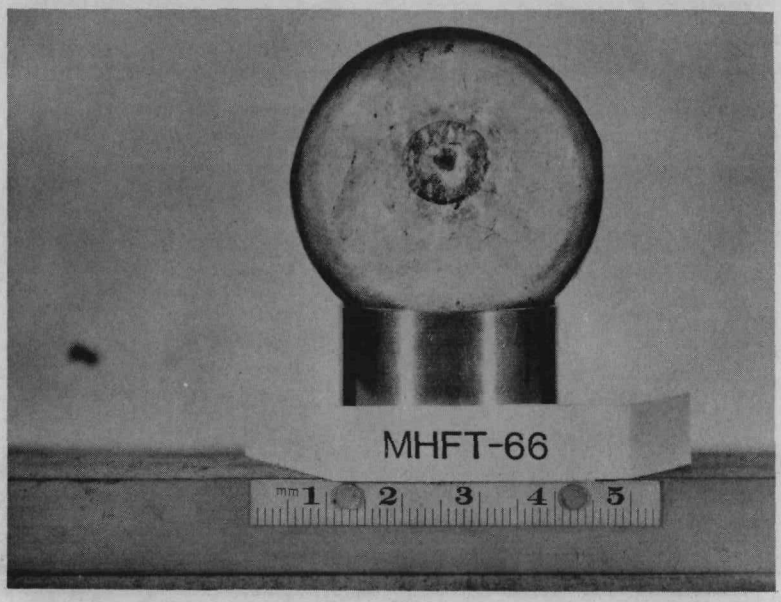

a. Impact

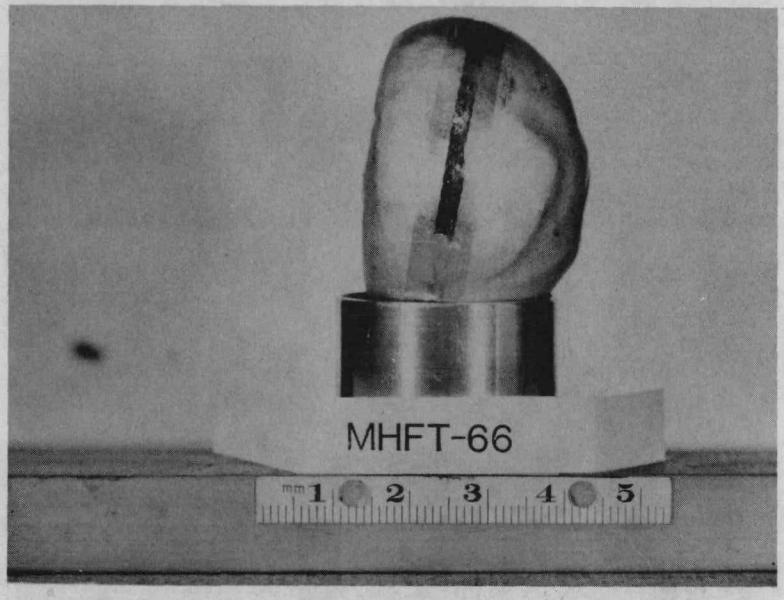

b. Profile

FIGURE 15. Impacted MHFT 66 (Photographs courtesy of D. Pavone, LANL[7])

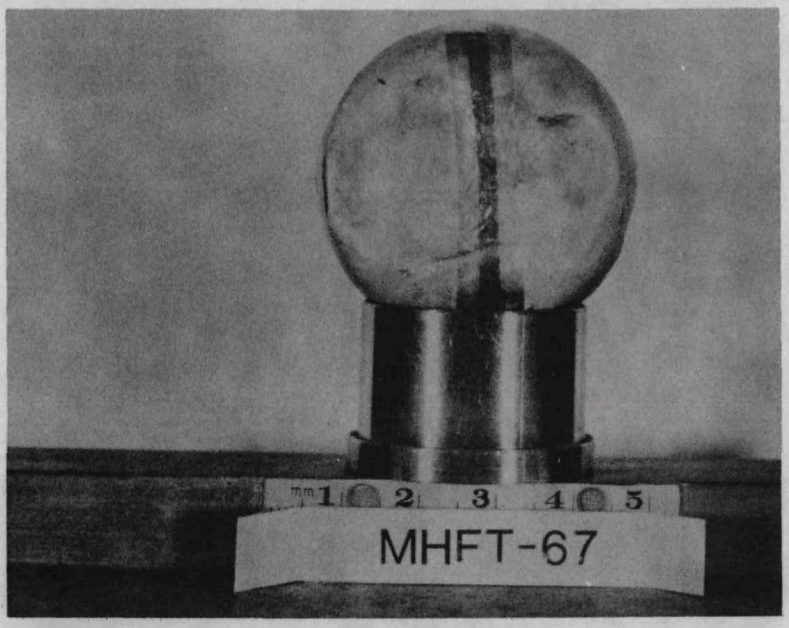

a. Impact Face

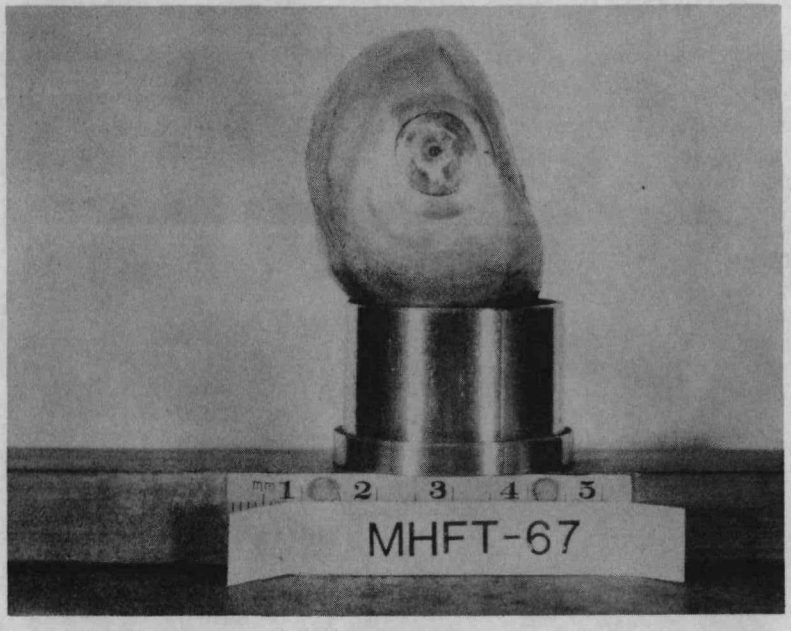

b. Profile

FIGURE 16. Impacted MHFT 67 (Photographs courtesy of D. Pavone, LANL[8])

a. Impact Face

b. Profile

FIGURE 17. Impacted MHFT 68 (Photographs courtesy of D. Pavone, LANL[9])

a. Impact Face

b. Profile

FIGURE 18. Impacted MHFT 69 (Photographs courtesy of D. Pavone, LANL[10])

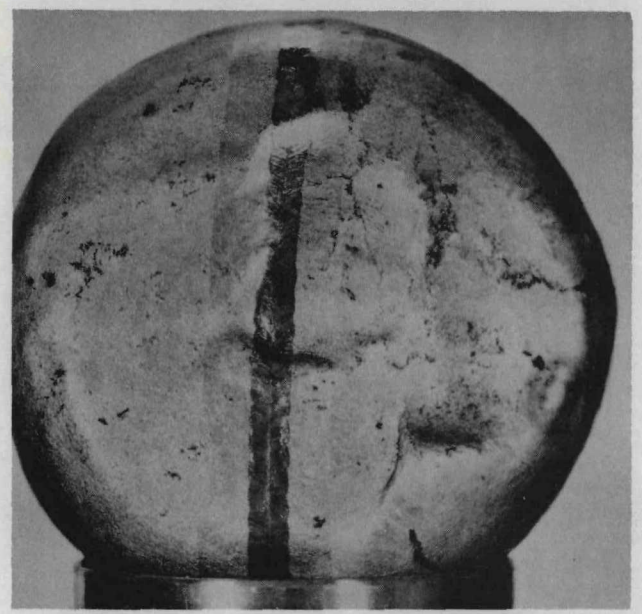

a. Impact Face

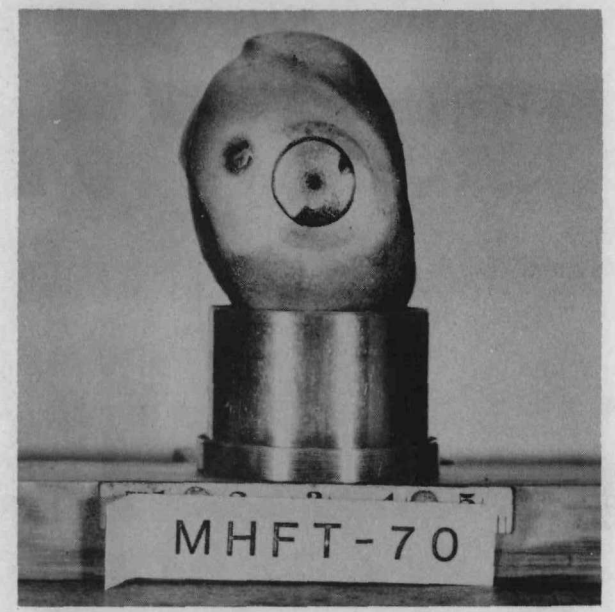

b. Profile

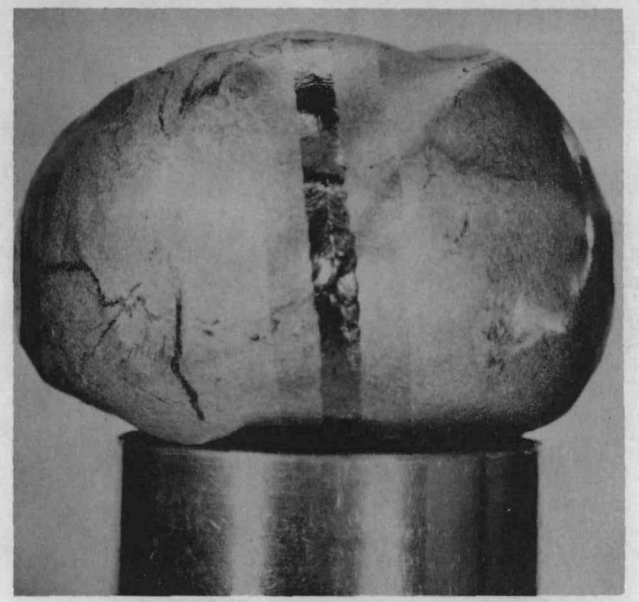

c. Profile

FIGURE 19. Impacted MHFT 70 (Photographs courtesy of D. Pavone, LANL[4])

TABLE 3

SVT Sample No.	SRP Sphere No.	Reference No.	Aging Conditions Time, hr	Aging Conditions Temp., °C	Impact Conditions Velocity, m/sec	Impact Conditions Temp., °C	Lobe-Type Push-Through	Failure Type Push-Through	Failure Type Fingerprint	Iridium Type
Preproduction Spheres										
MHFT-61	2	4	8834	1210	74.1	1440	Yes	No failure		DOP-26
MHFT-62	11	5	720	1210	85.0	1440	No	x	x	HDR
MHFT-64	17	6	720	1210	85.0	1300	No	-	x	DOP-26
MHFT-65	28	1	4400	1210	85.0	1440	Yes	x	x	DOP-26
MHFT-66	23	7	720	1210	85.0	1440	No	No failure		HD
Production Spheres										
MHFT-67	36	8	100	1200	82.9	1440	Partial	No failure		DOP-26
MHFT-68	37	7	110	1210	81.7	1579	No	No failure		DOP-26
MHFT-69	38	10	100	1210	82.2	1037	No	Re-entrant fold crack	x	DOP-26
MHFT-70	39	11	720	1210	82	1430	Partial	No failure		DOP-26
MHFT-72	64	12	720	1210	81.6	1430	No	No failure		DOP-26

a. Impact Face

b. Profile

FIGURE 20. Impacted MHFT 72 (Photographs courtesy of D. Pavone, LANL[11])

Summary and Conclusions

Failure of MHFT 65 focused attention on pre-impact fracture of the fuel into large integral chunks with subsequent sliding of these chunks over one another on impact as principal causes of fuel lobe-type push-through failure of the iridium. However, after available evidence was reconsidered, SRL concluded that:

(1) Lobe-type push-through failure of the spheres such as that seen on MHFT 65 is not caused by sliding of a large hard chunk of fuel along an existing crack. Instead, the pronounced lobes are presumably caused by sandbagging, or shear of loose and highly broken up pieces, of the fuel into the resultant gap following failure of the GIS. The inability of the iridium PICS for MHFT 65 to withstand the resultant strain was caused by phosphorus-induced embrittlement of the iridium.

(2) Impact behavior of MHW fuel should not be affected by pre-existing cracks in the fuel or large hard chunks as long as the GIS remains intact.

(3) If the GIS does fail and lobe-type push-through occurs, the presence of pre-existing cracks or hard chunks is not expected to necessarily make lobe-type push-through more or less pronounced or failure of the iridium more or less likely because the high degree of breakup of the fuel, regardless of original condition, is expected to cause the spheres to sandbag into the gap in about the same way.

These deductions are based on (1) evaluation of available LANL impact data, and (2) a computer modeling study performed by Fairchild Space & Electronics Co., Germantown, Maryland[3].

On the basis of the present failure model, catastrophic failure of future spheres will occur if all of the following conditions are met:

- The GIS must fail in such a way as to allow lobe-type push-through.
- Time of the GIS failure must be early in the impact event so that the PISA has sufficient energy left to deform into the gap.
- The iridium must respond in a brittle (rather than ductile) fashion.

Although the probability of another catastrophic failure can not be calculated, available data and recent SVT experience suggest that failure of MHFT 65 was an uncommon event.

The available data suggest that failure of MHFT 65 was due to failure of the GIS and was not product history dependent. For side-on impact of a GPHS fuel--which would have a circular cross section--application of the MHW failure mechanism is probably a good approximation. Therefore, any lobe type failure of iridium in side-on impacts of GPHS fuel should be the result of failure of the GIS rather than of effects of pre-existing crack networks in the fuel.

$^{238}PuO_2$ PROCESS DEVELOPMENT

DIRECT FABRICATION OF GPHS FUEL PELLETS USING Pu(III) DIRECT-STRIKE FEED

Summary

The feasibility of using a direct fabrication process to produce full-scale GPHS fuel pellets has been demonstrated. A GPHS pellet was successfully hot pressed using sintered "$^{242}PuO_2$"* rosettes as a feed material. These "$^{242}PuO_2$" rosettes were used as a simulant for Pu(III) direct-strike rosettes which have been produced on a laboratory-scale as described in a previous report.[12] This laboratory experiment also demonstrated that direct-fabrication pellets made from Pu(III) direct-strike feed have a microstructure and degree of cracking comparable to GPHS pellets made by the current process. Full-scale Pu(III) direct-strike oxalate precipitations are planned to help demonstrate that an acceptable feed for direct fabrication can be produced in production-scale tests.

Feed Material

Previously,[12] 60 to 100-μm spherical aggregates of PuO_2 crystals were produced by SRL using a two-step Pu(III) direct-strike precipitation process. Previous work also showed that these rosette-shaped aggregates could be densified to >95% theoretical density 9TD) by sintering for 6 hr at 1600°C in argon. A small-scale pellet fabrication test using these PuO_2 rosettes was also successful.

---

* Pu isotopic composition ~20% $^{240}PuO_2$ + ~80% $^{239}PuO_2$. This material was originally precipitated in JB-Line as feed for the SRP program for fabrication of reactor fuel tubes to be used to produce ^{242}Pu.

Full-scale Pu(III) direct-strike precipitation tests are planned to demonstrate this precipitation process in HB-Line and to provide $^{242}PuO_2$ rosettes were not immediately available in sufficient quantity to hot press full-scale GPHS pellets, a "simulant" material was needed to demonstrate the feasibility of full-scale pellet fabrication from a rosette-shaped feed material. Sufficient quantities of "$^{240}PuO_2$", known to have a rosette morphology, were available for fabrication tests.

SEM Characterization of the "$^{242}PuO_2$" rosettes indicated that this material was an adequate simulant for $^{238}PuO_2$ direct-strike rosettes. As shown in Figure 21, the "$^{242}PuO_2$" consisted of spherical aggregates, up to 120 μm in diameter but with a large volume of fines. Metallographic characterization indicated that "$^{242}PuO_2$" rosettes sintered in dry argon at 1600°C for 6 hr had a density of only about 85% TD (Figure 22a) while "$^{242}PuO_2$" rosettes sintered 6 hr at 1600°C in He/4% H_2 had a density >95% TD (Figure 22b). (A further discussion of atmosphere effects on granule densification will be discussed in alater quarterly report.)

Direct Fabrication (DF) Pellet 1

A full-scale GPHS pellet (Direct Fabrication (DF) Pellet 1) was fabricated using the "$^{242}PuO_2$" feed. The fabrication conditions and physical properties of DF Pellet 1 are reported in Tables 4 and 5. It was desirable to densify the granules prior to hot pressing to increase the pour density and to better duplicate the "grog" feed material presently being used in the GPHS process. Therefore, 50% of the granules were sintered at 1100°C in argon, and 50% of the granules were sintered at 1600°C in argon. As discussed earlier, the "$^{242}PuO_2$" rosettes had a density of only 85% TD after sintering 6 hr at 1600°C in argon. High-fired shards in the GPHS grog feed normally have a density of ~95% TD. The low-fired granules are very difficult to characterize, but the density and/or sinterability of the low-fired "$^{242}PuO_2$" granules may not have been the same as that of the low-fired shards in the GPHS grog feed.

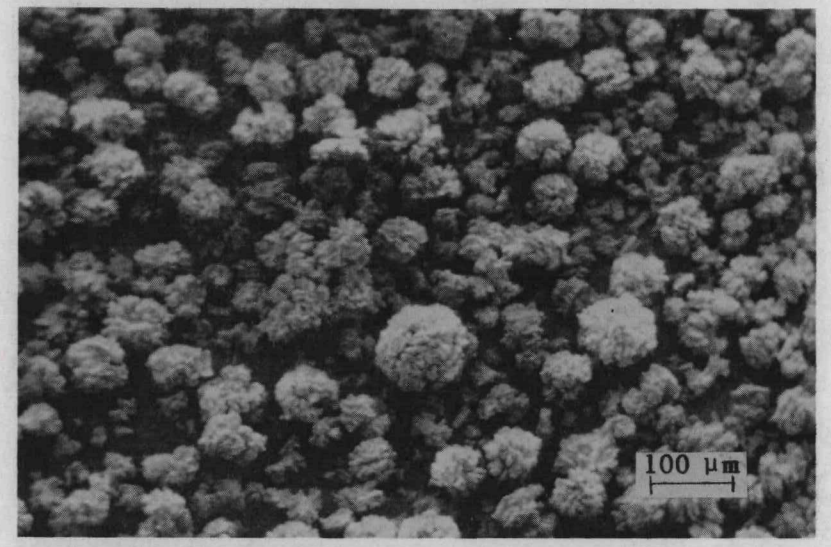

FIGURE 21. "$^{242}PuO_2$" Rosettes, As Received

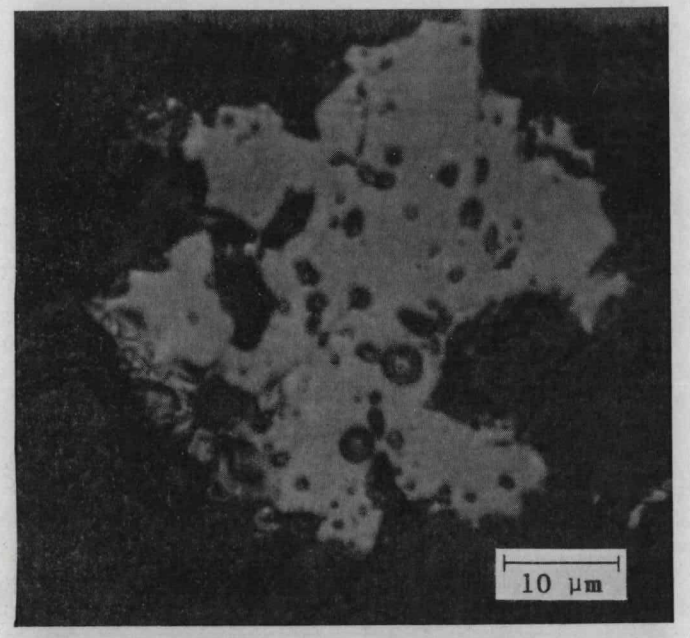

a. Granule Sintered 1600°C, 6 hr, Ar

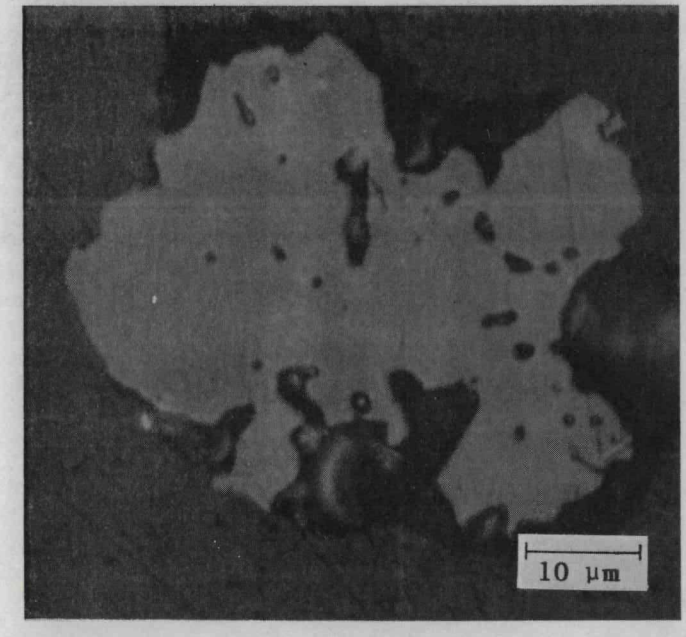

b. Granule Sintered 1600°C, 6 hr, He/4% H_2

FIGURE 22. Polished Sections of Sintered "$^{242}PuO_2$" Granules

TABLE 4

Process Conditions for Direct Fabrication Pellets

DF Pellet No.	Feed Material	Granules		Die Material	Hot Press Conditions		Heat Treatment
		Low-Fired	High-Fired		Pressure, psi	Temp., °C	
1	$^{242}PuO_2$	50% at 1100°C, 6 hr, Ar	50% at 1600°C, 6 hr, Ar	W-2% ThO_2	10,700	1615	1425°C, 6 hr, O_2
2	$^{242}PuO_2$	48% at 800°C, 6 hr, Ar	52% at 1600°C, 6 hr, He-4% H_2	Graphite	9300	1570	1525°C, 6 hr, O_2

TABLE 5

Physical Properties of Direct Fabrication Pellets

DF Pellet No.	Weight, g	Diameter, in.	Length	Density, % TD	Microstructure	Degree of Fracture
1						
AP	62.937*	-	-	-	High-density shell (2 mm wide)	Pellet broken during ejection from die liner, additional surface cracking after HT
HT	62.900*	-	-	-		
% Dif.	-0.06%	-	-	-		
2						
AP	148.706	1.0830	1.0810	84.5	Uniform density	Small, hairline cracks after HT
HT	149.420	1.0814	1.0836	85.0		
% Dif.	+0.48%	-0.15%	+0.24%	+0.5		

* Section of pellet

These differences in the granule feed material were the likely causes for the relatively high temperature (1615°C versus a GPHS centerline temperature of 1525°C) and pressure (10,700 psi versus a GPHS centerline condition of about 2700 psi) required to hot press DF Pellet 1. It should also be noted that DF Pellet 1 was hot pressed in a W-2% ThO_2 die[12] and that this test apparently exceeded the physical limitations of the die. As discussed in a previous report, DF Pellet 1 had broken when the die liner fractured during pellet extraction. Additional surface cracks formed in the piece which was heat treated. As shown in Figure 23, the metallographic examination of a section from DF Pellet 1 revealed a clearly defined, high-density (~98% TD) outer shell which was ~2 mm wide. The density of the remainder of the pellet was ~83 to 85% TD and fairly uniform. The high-density shell may have been related to the characteristics of the granules and/or the hot pressing parameters.

DF Pellet 2

The conditions used to sinter the granules for DF Pellet 2 were adjusted (Table 4) to produce denser, high-fired granules and more-sinterable, low-fired granules. These changes in granule sintering conditions helped reduce the pressure and temperature required to hot press the pellet. The pellet had no visible surface cracks following heat treatment (Figure 24). On the basis of microstructural analysis (Figure 25), the change in process conditions apparently helped to alleviate density gradients. There was no evidence of a high-density shell in DF Pellet 2 although a slightly higher density was observed near the side of the pellet than at the ends or center of the pellet. Some cracking, probably from reoxidation stresses, was also observed in a section of the pellet cut from near the side of the pellet.

It should also be considered that a graphite die, rather than W-2% ThO_2, was used to hot press DF Pellet 2. This may have contributed to some of the processing and microstructural differences, but there was no evidence to substantiate this possibility.

Conclusions

The microstructure and degree of fracture characteristic of pellets hot pressed from direct-strike rosettes is very similar to that of GPHS pellets. The similarities in granule size, pore size, grain size, and especially cracking, indicate that similar impact behavior should be expected.

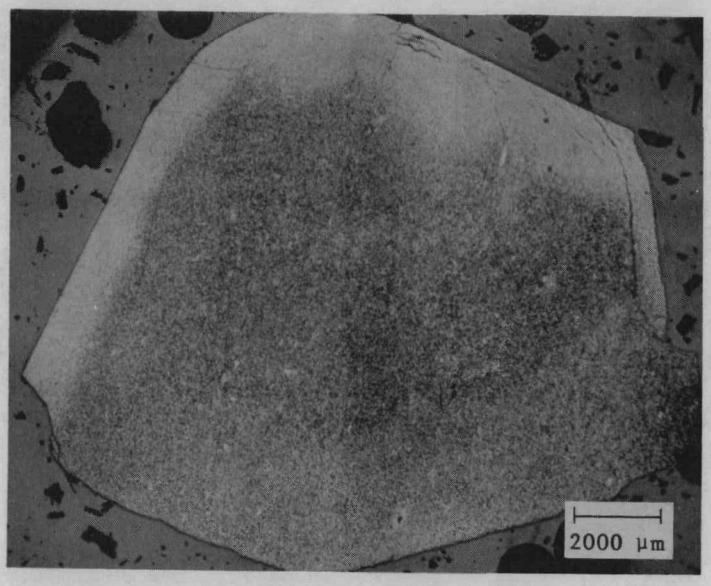

Polished Section

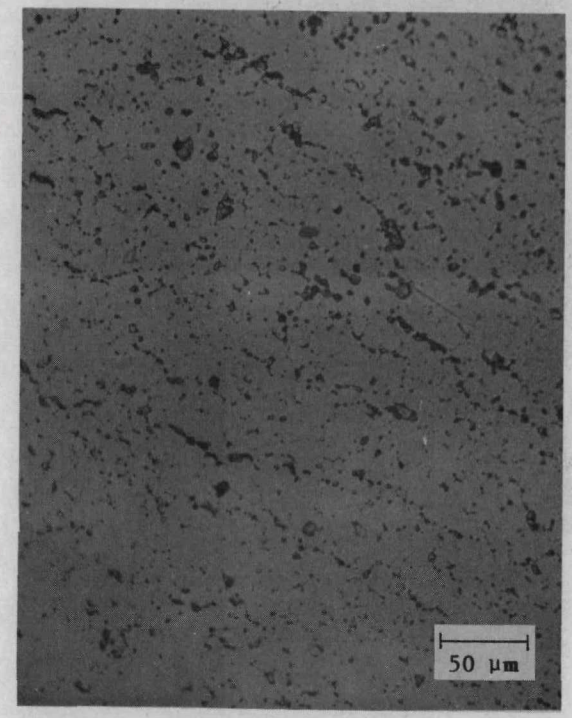

High-Density Shell

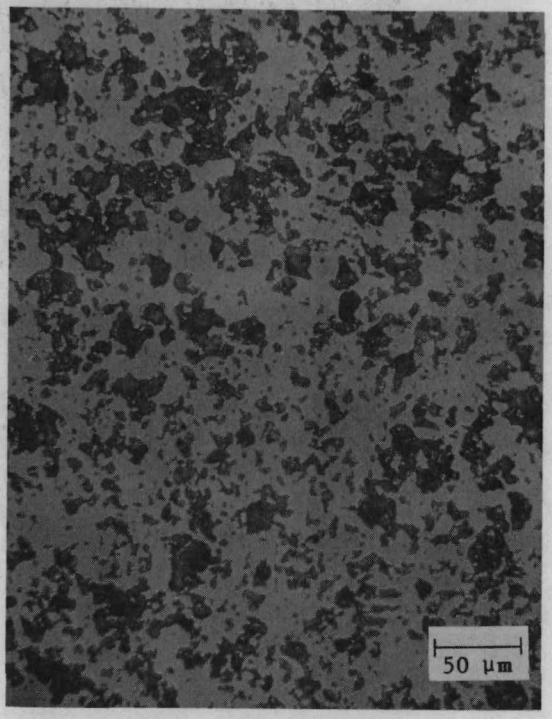

Low-Density Interior

FIGURE 23. DF Pellet 1

A proposed process flowsheet for the direct fabrication of $^{238}PuO_2$ fuel forms is presented in Figure 26. This flowsheet is only preliminary, since no full-scale direct fabrication tests have yet been made with $^{238}PuO_2$.

Program

Direct-strike precipitations of Pu(III) material in the HB-Line using two different procedures have been requested. The material from these precipitations will be characterized by SEM analysis and granule sintering studies to determine whether the feed is acceptable for direct fabrication. If the feed is acceptable, it will be hot pressed in the PEF to complete full-scale demonstration of the direct fabrication process.

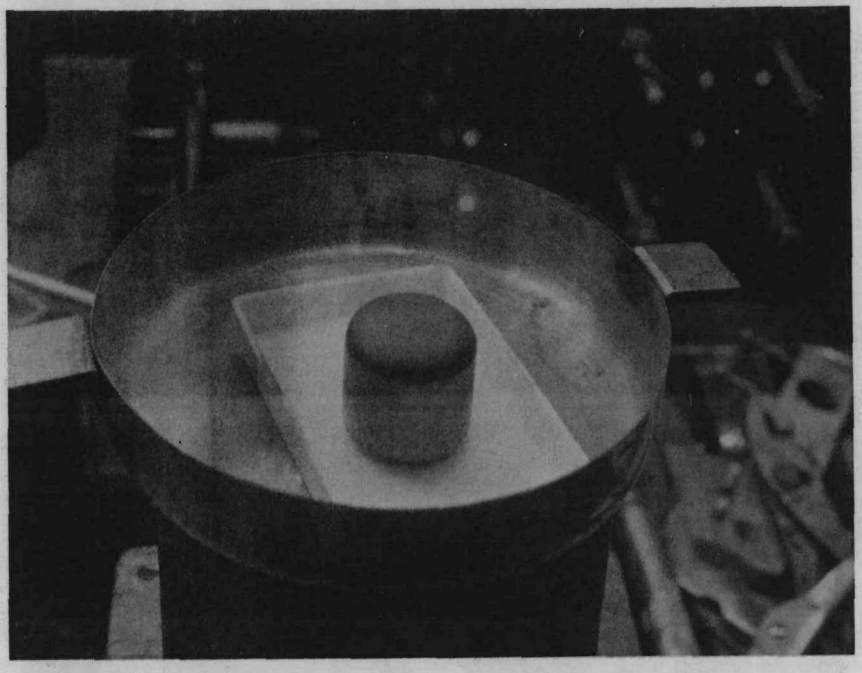

FIGURE 24. DF Pellet 2 After Final Heat Treatment

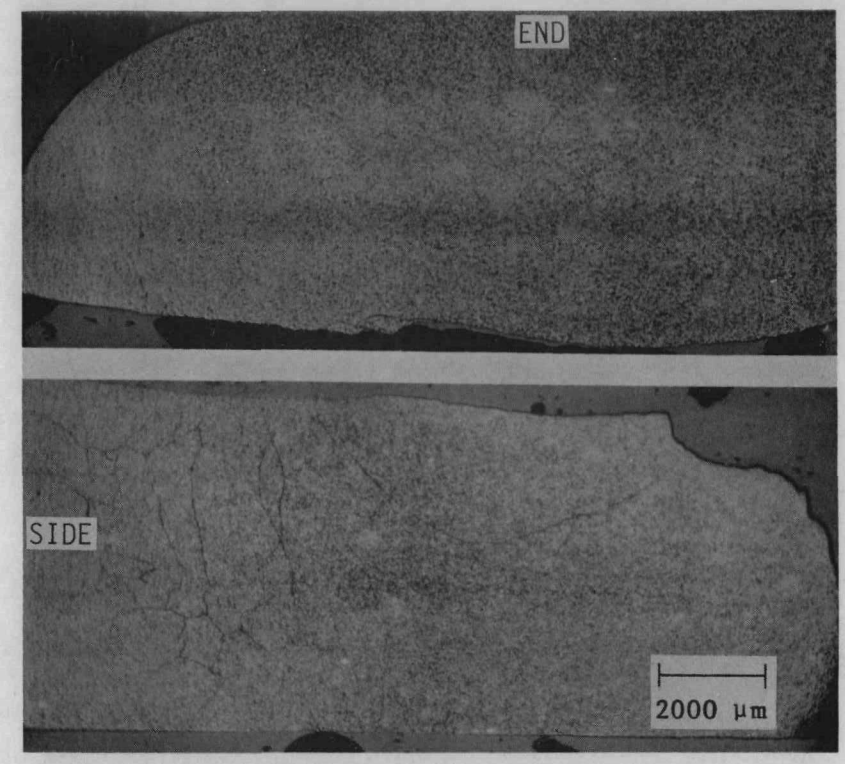

Polished Sections

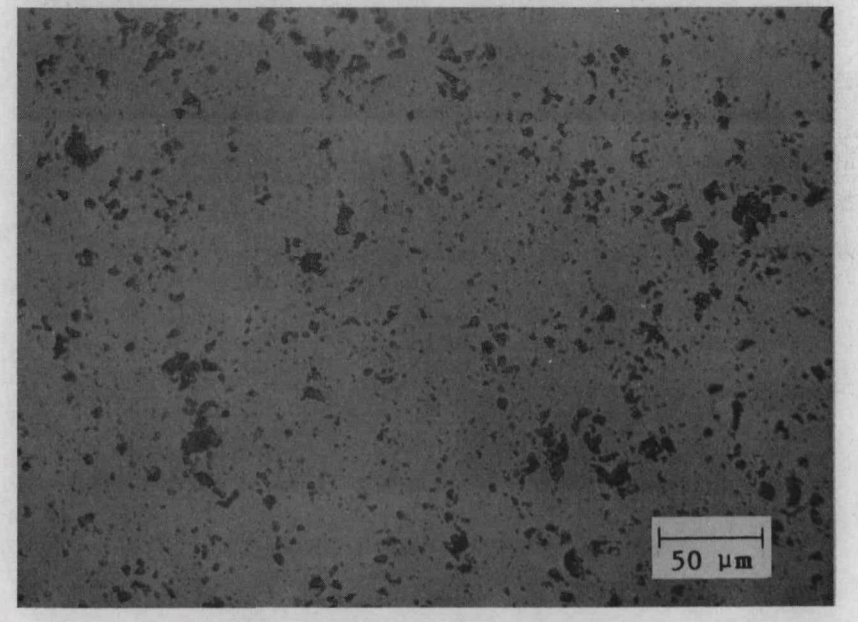

Typical Microstructure

FIGURE 25. DF Pellet 2

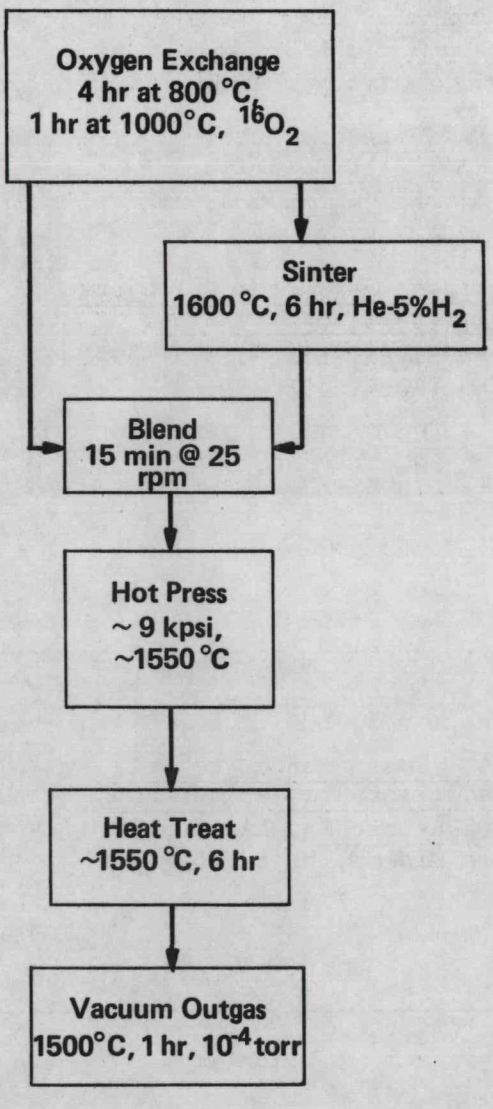

FIGURE 26. Proposed Process Flowsheet for the Direct Fabrication of $^{238}PuO_2$ Fuel Forms

REFERENCES

1. W. J. Maraman, Compiler. General-Purpose Heat Source Project, Space Nuclear Safety Program, and Radioisotopic Terrestrial Safety program, September 1979. USDOE Report No. LA-8150-PR, Los Alamos Scientific Laboratory, Los Alamos, NM 87545 (November 1979).

2. Multi-Hundred Watt Radioisotope Thermoelectric Generator Program: 1976-1977 Annual Report/Final Report for the Voyager Program. USDOE Report No. GESP-7134, GEMS-430, Section 5, General Electric Co., Philadelphia, PA (1977).

3. W. J. Maraman, Compiler. General-Purpose Heat Source Project and Space Nuclear Safety and Fuels Program, January 1980. USDOE Report No. LA-8311-PR, Los Alamos Scientific Laboratory Los Alamos, NM 87545 (April 1980).

4. W. J. Maraman, Compiler. General-Purpose heat Source Project and Space Nuclear Safety and Fuels Program, August 1980. USDOE Report No. LA-8713-PR, Los Alamos Scientific Laboratory, Los Alamos, NM 87545 (January 1981).

5. R. P. Swift, R. Brown, K. Wahi, and M. B. Eck. Fuel Sphere Assembly Deceleration Behavior During Impact: Calculations and Analyses. USDOE Report No. FSEC-ESD-217-75-63P, Fairchild Space & Electronics Company, Germantown, MD (October 1975).

6. R. D. Baker, Compiler. Gneral-Purpose Heat Source Project, Space Nuclear Safety Program, and Radioisotopic Terrestrial Safety Program, February 1979. USDOE Report No. LA-7805-PR, Los Alamos Scientific Laboratory, Los Alamos, NM 87545 (April 1979).

7. W. J. Maraman, Compiler. General-Purpose Heat Source Project, Space Nuclear Safety Program, and Radioisotopic Terrestrial Safety program, April 1979. USDOE Report No. LA-7868-PR, Los Alamos Scientific Laboratory, Los Alamos, NM 87545 (June 1979).

8. W. J. Maraman, Compiler. General-Purpose Heat Source Project and Space Nuclear Safety and Fuels Program, February 1980. USDOE Report No. LA-8386-PR, Los Alamos Scientific Laboratory, Los Alamos, NM 87545 (May 1980).

9. S. E. Bronisz, Compiler. Space Nuclear Safety and Fuels Program, November 1980. USDOE Report No. LA-8735-PR, Los Alamos Scientific Laboratory, Los Alamos, NM 87545 (February 1981).

10. W. J. Maraman, Compiler. General-purpose Heat Source Project and Space Nuclear Safety and Fuels Program, July 1980. USDOE Report No. LA-8582-PR, Los Alamos Scientific Laboratory, Los Alamos, NM 87545 (October 1980).

11. W. J. Maraman, Compiler. General-Purpose Heat Source Project of Space Nuclear Safety and Fuels Program, September 1980. USDOE Report No. LA-8714-PR, Los Alamos Scientific Laboratory, Los Alamos, NM 87545 (January 1981).

12. ^{238}Pu Fuel Form Processes Quarterly Report January - March 1980. USDOE Report No. DPST-80-128-1, E. I. du Pont de Nemours & Co., Savannah River Laboratory, Aiken, SC 29808 (1981).

13. ^{238}Pu Fuel Form Processes Quarterly Report July-September 1980. USDOE Report No. DLPST-80-128-3, E. I. du Pont de Nemours & Co., Savannah River Laboratory, Aiken, SC 29808 (1981).

DISTRIBUTION DPST-80-128-4

Copy No.

1 N. Goldenberg, Director, Office of Advanced Nuclear Systems and Projects, U. S. Department of Energy

2 B. J. Rock, Director, Space and Terrestrial Systems Division, Office of Advanced Nuclear Systems and Projects, U. S. Department of Energy

3 J. J. Lombardo, Acting Chief, Power Systems Branch, Space and Terrestrial Systems Division, U. S. Department of Energy

4 G. Bennett, Acting Chief, Safety and Isotope Fuels Branch, Space and Terrestrial Systems Division, U. S. Department of Energy

5. D. Sewell, Asst. Secretary for Defense Programs, U. S. Department of Energy

6. A. W. Whiteman, Albuquerque Operations Office

7. D. L. Krenz, Albuquerque Operations Office

8. H. N. Hill, Manager, Dayton Area Office

9. R. D. Baker, CMB, DO, Los Alamos National Laboratory

10 S. E. Bronisz, CMB-5, MS-730, Los Alamos National Laboratory

11 R. A. Kent, Los Alamos National Laboratory

12 R. Behrens, Los Alamos National Laboratory

13 W. T. Cave, Monsanto Research Corporation

14 B. R. Kogenge, Monsanto Research Corporation

15 Technical Library, Sandia National Laboratories, Albuquerque

16 M. K. Parson, Sandia National Laboratories, Albuquerque

17 T. J. Young, Sandia National Laboratories, Albuquerque

18 W. Whitmore, General Electric Company, Philadelphia

19 R. H. Cooper, Oak Ridge National Laboratory

20 W. Pardue, Battelle Memorial Institute, Columbus, Ohio

21-26 Savannah River Operations Office, DOE

27-64 Savannah River Laboratory, TIS Files

65-66 Technical Information Center, Oak Ridge, TN

67 G. Linkous, Teledyne Energy Systems, Timonium, MD